Royal Netherlands
Meteorological Institute
Ministry of Infrastructure
and Water Management

Utrecht University

MASTER THESIS

BLACKOUTS ARE NOT AN OPTION

Or a study of extreme weather and high impacts in compound energy production and energy shortage

Author:
Laurens P. STOOP BSc
Study: Climate Physics
Student nr.: 3986209

Daily supervisor:
Dr Karin VAN DER WIEL
Royal Netherlands Meteorological Institute

Supervisor:
Dr Aarnout VAN DELDEN
Institute for Marine and Atmospheric Research Utrecht

Supervisor:
Prof. Dr Michiel R. VAN DEN BROEKE
Institute for Marine and Atmospheric Research Utrecht

UTRECHT UNIVERSITY

6 July 2018

Cover image: Florian Juengermann, Germany 28 November 2017 / CC0 Creative Commons

Abstract

This thesis characterizes the meteorological weather patterns leading to high societal impact. High societal impacts can be either due to low compound wind and solar energy production, or due to high energy shortage.

The share of renewable energy, like wind and solar energy, in the electrical grid, will likely increase as mitigation measures for future climate change are put into effect. Renewable energy production is largely dependent on the variability of the weather and is thus subject to variability on all timescales. This variability can be partly compensated for by integrating the wind and solar energy resources over a large area. However, the weather not only affects the production of renewable energy, but also the energy demand.

For this study we use 2000 years of simulated daily meteorological conditions to calculate 2000 years of daily compound wind and solar energy production, based on a projected distribution of renewable energy sources, to calculate 2000 years of projected daily energy demand and shortage. Meteorological input data are generated with the global climate model EC-Earth V2.3. The selection of the high-impact events is based on the highest societal impact rather than on the extremeness of a chosen meteorological variable.

It is found that the 1-in-10 year highest impact events for one-day low compound energy production are extended high-pressure systems in winter over central Europe, causing low wind speed conditions with minimal incoming solar radiation. Of these events only 1% is also considered as a high-impact event on a weekly timescale, as the very stationary and persistent high-pressure systems needed are only observed in the summer. For 1-in-10 year high energy shortage events the weather patterns are characterized by a similar high-pressure system, but situated a bit more to the north and accompanied by anomalously cold temperatures throughout the region. Of these events, 13.5% is also the determinative high-impact event on a weekly timescale. For both low compound energy production and high energy shortage the highest daily societal impact extremes are found to not be the same as the impact caused by the most extreme weather conditions. Assuming no changes in the distribution of renewable energy sources and with a constant temperature dependency of demand, the change in the occurrence of the highest societal impact events for energy shortage is found to be much smaller then the signal found due to inter-model differences.

Preface

Before you lies the master thesis, "Blackouts are not an option; or, a study of extreme weather and high impacts in compound energy production and energy shortage." The basis of the research was the HiWAVES3 dataset that is used to study high-impact weather events all over the world. This master thesis is written to fulfil the graduation requirements of the Climate Physics master at Utrecht University. I worked on the research from November 2017 until July 2018 at the Royal Dutch Meteorological Institute.

What started out as a study into renewable energy extremes and how weather affects these events, turned into a more elaborate research that also includes an estimation of energy demand, as this would allow the shortage of energy to be studied as well. The reason for this extension was the fact that weather not only affects the production of renewable energy, but also the energy demand. This extension of what is considered an impact extreme, forced me to focus less on the risk and recurrence of these extreme impact events and more on a characterization of the meteorological conditions.

The contents of this master thesis are very relevant for all those who are interested in high-impact weather events, the study of energy compound extremes, or the risk associated with renewable energy sources. For those with a background in Climate Physics some insight into the high non-linearity of certain impacts and their relation to climate variability can be obtained. The implications of the results of this thesis are of special interest for those who are interested in the transition towards renewable energy.

I would like to thank my supervisor, Dr Karin van der Wiel for the considerable time she took for discussion and guidance during my research. I would also like to thank all those who worked with me on this project and commented on my process, method and code.

I hope you enjoy your reading.

Laurens Stoop
De Bilt, 2018

Contents

1 Introduction

1.1 Challenges for future energy safety

The share of renewable energy in the electrical grid will likely increase as mitigation measures for future climate change are put into effect [International Energy Agency, 2017]. Renewable energy production, such as wind and solar energy, is largely dependent on the weather conditions and is thus subject to variability on all timescales, see [Chiacchio and Wild, 2010], [Hedegaard and Meibom, 2012], [Pryor et al., 2006], [Staffell and Pfenninger, 2016], [Brayshaw et al., 2011] and [Jerez et al., 2013]. This sensitivity of the power system to meteorological drivers is expected to increase, due to the increasing share of renewable energy sources [Bloomfield et al., 2016], [International Energy Agency, 2017]. As generation has to be matched to demand, dealing with this variability is the main challenge for future energy safety. Different methods can be used to match the variable supply with a fixed demand, the two most used of which will be explained here.

One method for reducing the impact of meteorological variability is by using novel energy storage technologies, to store enough energy in times of high production to compensate for periods of scarcity. However, most techniques are currently limited to short timescales in practical applications [Ferreira et al., 2013], [Díaz-González et al., 2012] and [EPRI, 2010]. A lot of effort is going into finding long-term storage solutions [Blanco and Faaij, 2018], but very few of these are currently cost-effective [Staffell and Rustomji, 2016], [Gabrielli et al., 2018].

A second method for reducing variability is based on the idea that weather patterns are limited in size and that therefore the energy required to match demand can be generated outside of the obstructing weather pattern and transported to where it is needed. To achieve this the variable renewable energy sources need to be integrated over a large area to reduce the sensitivity to local meteorological conditions. See Giebel [2000] for some early work on this method, for recent work see Monforti et al. [2016], Ravestein et al. [2018] and Tobin et al. [2018]. The development of a projection for an integrated, large-scale approach for the deployment of renewable energy in Western Europe is the subject of current research by *B. van Zuijlen* and *M. van den Broek*.

Reanalysis data is generally used to study the meteorological dependency and determine the best placement of renewable energy sources. [Cradden et al., 2017], [Jerez et al., 2015], [Bett et al., 2013] and [Bloomfield et al., 2018]. This limits the research to observed weather events in the recent past [Dee et al., 2011] and limits the sampling of extreme conditions. Consequently, the full range of possible weather patterns is hereby underestimated [Cannon et al., 2015]. To better sample the full variability of the climate system, (regional) climate simulations can be used, see [Ravestein et al., 2018], though biases and modelling errors do need to be taken into account.

In an energy system where only a small part of the energy production is done by variable renewable energy sources the undersampling of extreme societal impact events, like a system blackout, is not considered a big issue, as there is enough traditional (fossil fuel or nuclear-based) back-up power in the system [Hedegaard and Meibom, 2012] to match energy demand and generation. However, as stated before, the share of renewable energy in the electrical grid will likely increase and as the share of renewable energy grows we will become more vulnerable to a change in the frequency and occurrence of these extreme societal impact events, see [Ravestein et al., 2018] and [Koch et al., 2015].

That relying on even a small share of renewable energy can threaten grid stability became apparent on the 30th of April 2018 in the Netherlands. On that day an unusually small, less

than 10%contribution of variable renewable energy caused a lot of problems as no renewable energy was produced at all that day due to a small shift in the weather pattern. Consequently, large amounts of energy needed to be brought in from Belgium and Germany to maintain grid stability, see [NOS, 2018] and [Koster, 2018]. A similar sudden strong reduction in renewable energy production was also found in a case study on the electricity grid in Great Britain. There it was found that variable renewable energy sources are extremely sensitive to meteorological drivers on a local scale [Bloomfield et al., 2018].

1.2 High impacts and extreme weather

In current climate impact and risk studies a large focus is placed on extreme weather. As a first indicator one might indeed guess that extreme weather causes extensive damage and therefore also causes the highest societal impacts. However, the spatio-temporal interaction between meteorological variables and specific combinations of weather events, can also cause high societal impacts due to complex non-linear interactions [van der Wiel et al., 2018]. For this reason, when studying societal risk, it is important to focus on the highest impacts and not on the most extreme weather events, see [Zscheischler et al., 2018] and [van der Wiel et al., 2018]. Only a direct calculation of impacts can guarantee that the right extreme events are selected. The use of this novel approach to determine high-impact events is currently limited. Research into these compound events currently focusses on coastal flooding, heat stress and storm damages [Zscheischler et al., 2018], but not on the energy sector and the future energy safety.

The impact of the variability of weather on renewable energy production and energy shortage is the subject of ongoing research, see [Davy et al., 2017], [Grams et al., 2017], [Hueging et al., 2013], [Pozo-Vázquez et al., 2004], [Ravestein et al., 2018] and [Tobin et al., 2016]. However, these studies focus on the impacts caused by specific weather patterns and modes of the climate system, rather than the societal impact itself. As shown by [Bloomfield et al., 2018], the complicated and non-linear coupling between meteorological variables and renewable energy make the energy grid susceptible to high-impact events. Therefore, ongoing and future research into impacts of meteorological conditions should focus on the societal impact of weather rather than extremeness of weather, if it is to capture the right impact extremes.

1.3 The aim of this thesis

While mitigation measures to battle climate change drive the demand for renewable energy sources, the weather-induced variability for a high share of renewable energy sources into our electricity grid is still largely unknown. In this study 2000 years climate simulation data on a daily resolution from the HIWAVES3 project and the projected distribution of variable renewable energy sources for Western Europe developed by *B. van Zuilen* and *M. van den Broek* will be used to answer the following question:

What are the meteorological conditions that lead to periods with high societal impact due to the use of renewable energy?

In answering this question two impact measures will be used: compound energy production and energy shortage. Compound energy production is defined here as the region-wide daily total energy production from utility-scale solar power plants, rooftop solar panels, off- and onshore wind turbines combined. Energy shortage is defined here as the difference between energy demand and the compound energy production. For the purpose of this study it is assumed that the entire Western European region can be considered to be a copperplate. Meaning that the total energy demand and compound energy production of the different countries can be shared without any loss over the full region and without considering any transport limitations.

High societal impact events are defined as the 1-in-10 year events with the highest impact. To identify these events the lowest compound energy production or the highest energy shortage are selected, as these have the potential of the most extreme societal impacts. The selection of

these high-impact events is done after direct calculation of the impact, to guarantee that the right high-impact events are selected from the full distribution of impacts.

To answer the main research question stated above we will first determine for both compound energy production and energy shortage:

- how their respective composition changes the selected high impact events,
- how extreme meteorology and high societal impact are related,
- what the meteorological conditions of the high-impact events are, and
- how the meteorological conditions change for different durations of high-impact events.

1.3.1 Outline thesis

In Chapter 2 I will explain the method used for modelling renewable energy production and demand. The climate model input data and the specific distributions of the four renewable energy sources used will also be discussed. Chapter 3 and Chapter 4 will then discuss the results obtained during the research. The structure of these chapters is the same to allow for easy comparison. Both chapters consist of four sections, dealing with the four sub-questions of my research. An initial look into the robustness of the results and its qualitative validity is presented in Chapter 5. In Chapter 6 the conclusions of this research are presented.

2 Impact model method

In this chapter the impact models used in this study are described. The goal of the impact models presented here is to translate climate data to societal impact parameters. Two impact parameters are used in this study. The first is compound energy production, the modelling of which will be explained in section 2.1. The model for the second impact parameter, energy shortage, is explained in section 2.2. The large climate model ensemble on which the two impact models are applied to obtain data on the impact parameters is described in section 2.3. The three limiting factors in this study on the impact parameters are discussed in section 2.4.

2.1 Modelling energy production

To calculate the compound energy production impact parameter, the energy production from each renewable energy source should be determined. Before we describe how the compound energy production impact parameter is calculated (section 2.1.5), we describe how energy production is modelled. (WHY DO YOU SUDDENLY USE "WE"?)

The method used here to calculate the renewable energy production is the same method that was used by Jerez et al. [2015] and Ravestein et al. [2018]. It allows for an integral approach, because the model is similar for different renewable energy sources. This is why it is usually the preferred model for research applications.

The calculation of the energy production (P_{RES} in TWh/day) is split into three independent puzzle pieces (equation (2.1.1)): the calculation of the energy potential (RES_{pot}, a scalar), installed capacity (IC_{RES} in TW), and operational time (t_{oper} in h/day). These three quantities need to be solved for each source of renewable energy to determine their respective energy production.

$$P_{RES}(t) = RES_{pot}(t) \times IC_{RES} \times t_{oper} \tag{2.1.1}$$

In section 2.1.1 and 2.1.2 we will explain the calculation of the energy potential for wind and solar energy sources. The deployed capacity of the renewable energy sources used in this study will be explained in section 2.1.3. In section 2.1.4 we will discuss the considerations that have to be made to calculate the operational time. Figure 2.1 shows a flowchart of how the different data variables are combined in the calculation of the daily compound energy production.

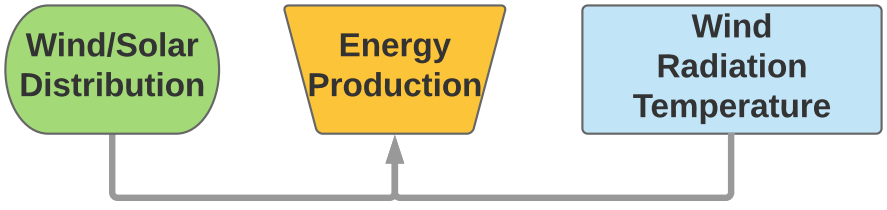

Figure 2.1 – Flowchart of the calculation method for daily compound energy production. In green the spatial distribution data, in blue the climate variables used, and in orange the compound energy production is shown.

2.1.1 Wind energy potential

The first piece of the puzzle in determining the energy production from a wind energy source is the wind energy potential. The calculation of the time-dependent wind energy potential is a two-step process. First the wind speed needs to be scaled from the modelled 10 metre height to the hub-height of the wind turbines, as the wind speed at hub-height is not calculated in the climate simulations. Then, using this wind at the hub-height and a so-called power curve, the wind energy potential at each time step can be calculated. The hub-heights used in this study are 80 and 120 metres for the respective on- and offshore wind turbines, see 2.1.3.

Scaling the wind speed to hub-height

For the scaling of the wind speed two different methods can be used, the wind speed can be scaled to the hub-height with the logarithmic profile, or with the empirical power law. The logarithmic wind profile gives accurate wind speeds at height, but only if the boundary layer properties are known [Davy et al., 2017]. This means that additional information on the surface wind stress, local air density and the frictional properties of the boundary layer is needed for this method to work. For the power law profile, the only additional information needed is the roughness parameter (also known as the Hellmann exponent). As Hsu et al. [1994] showed, and was reaffirmed by Emeis and Turk [2007], the power law is more accurate in practice than the logarithmic wind profiles upwards of 80 metres, because frictional properties like the surface roughness length and Monin-Obukhov-Length are very difficult to determine accurately. For these two reasons reason the empirical power law profile is used in this study to scale the modelled 10 metre wind speed to the wind speed at height.

The empirical power law is given by equation (2.1.2) and shown in figure 2.2. Using the empirical power law the wind is scaled to the hub-heights used.

$$V(h) = V(h_0)\left(\frac{h}{h_0}\right)^{\alpha} \tag{2.1.2}$$

In which $V(h)$ is the wind at height in m/s, h is the hub-height in metres, h_0 is the reference height in metres (10 metres in our study) and α is the roughness parameter. The roughness parameter for onshore regions is set to $\alpha = 0.143$ and for offshore regions the roughness parameter is set to $\alpha = 0.11$ [Hsu et al., 1994], [Akpinar and Akpinar, 2005].

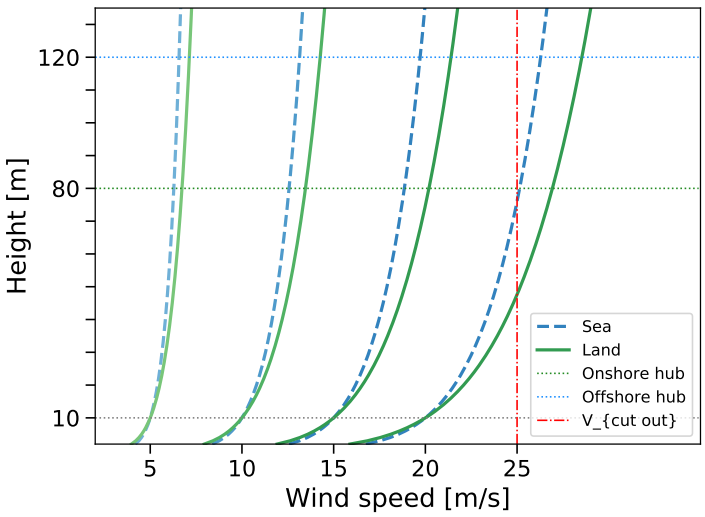

Figure 2.2 – The power law wind profile is shown for different 10 metre wind speeds for onshore regions $\alpha = 0.143$ in green and for offshore regions $\alpha = 0.11$ in dashed blue lines. The hub-heights used are shown as grey dotted lines.

Wind power curve modelling

One of the major factors that affect wind turbine output is the non-linear dependence of energy production on wind speed, see figure 2.3. The characteristic wind speeds for this non-linear dependence are the cut-in wind speed ($V_I = 3.5$ m/s), the rated wind speed ($V_R = 13$ m/s) and the cut-out wind speed ($V_O = 25$ m/s). The exact value of these wind speeds can be changed to maximize the power output of a specific site and turbine. The three characteristic wind speeds define four performance regions, that together define the power curve of a wind turbine. These four different performance regions are shown in figure 2.3. For a more extensive discussion on the different regions and more details on the physical basis of the regions see chapter 5 of *Wind energy: Fundamentals, resource analysis and economics* by Mathew [2007].

The critical issue in modelling the output of a wind turbine is the behaviour of a wind turbine in the second region, as regions one, three and four have constant wind power potential [Carrillo et al., 2013], [Mathew, 2007]. Typically this so-called power curve data is provided by the manufacturer of a wind turbine and is usually a piecewise function that is unique to a specific wind turbine [Mathew, 2007] and therefore useless when studying a collection of different wind turbines, or when making projections for the future. To determine the best modelling method for the behaviour of a wind turbine, Carrillo et al. [2013] reviewed the four most common methods of power curve modelling and they found that both the exponential and the cubic approximation of the power curve give a good estimate. As the cubic equation method requires some knowledge of the exact wind turbine, the exponential power curve method was used in this study, because we use a projected distribution of wind turbines.

The exponential power curve model is given by formula (2.1.3), shown here in the style of **?**. The formula shown is mathematically the same as Mathew [2007] and Carrillo et al. [2013], but rewritten to allow for better interpretation.

$$W_{pot} = \begin{cases} 0 & if \quad V < V_I, \\ \frac{V^n - V_I^n}{V_R^n - V_I^n} & if \quad V_I \leq V < V_R, \\ 1 & if \quad V_R \leq V < V_O, \\ 0 & if \quad V \geq V_O \end{cases} \tag{2.1.3}$$

where W_{pot} is a scalar indicating the renewable energy source potential (RES_{pot}), V is the wind speed in m/s at hub-height and $n = 3$ is the ideal velocity power proportionality. Lower values of n are sometimes used to compensate for the energy loss in the gearing of a wind turbine.

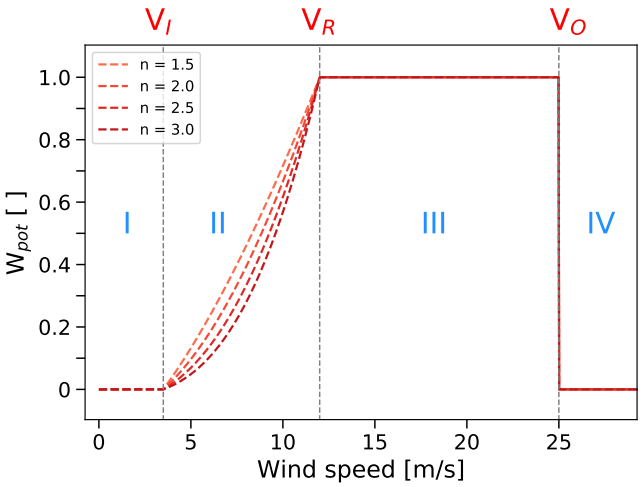

Figure 2.3 – The wind generation profile is shown for different velocity power proportionality factors n. The different performance regions are indicated by Roman numerals and the characteristic wind speeds are indicated above.

2.1.2 Solar energy potential

The first piece of the puzzle in determining the energy production of a solar energy source is the solar energy potential. Due to the high industrialization of solar panel production, the modelling of the power output for a solar panel is split into two parts: the weather dependency and the solar panel design. The solar panel design part is quite simple, as it only requires changing the installed capacity in formula (2.1.1) to the installed nominal power. The weather dependent part is then given by equation (2.1.4). See Mavromatakis et al. [2010] and Jerez et al. [2015] for the steps as they are used here, for a more detailed study on the solar potential of a site see Chenni et al. [2007].

$$PV_{pot} = P_R \frac{I}{I_{std}} \tag{2.1.4}$$

where PV_{pot} is a scalar indicating the renewable energy source potential (RES_{pot}), I is the short-wave downward radiation at the surface in W/m^2, I_{std} is the standard test condition for solar photovoltaic cells ($I_{std} = 1000$ W/m^2) and the performance ratio is given by P_R.

The performance ratio can be defined in three distinct ways [Jerez et al., 2015]. It can be defined as a constant value, it can be a function of the solar cell temperature, or it can be a function of the solar cell temperature after wind induced cooling has been taken into account. As was found by TamizhMani et al. [2003] and reaffirmed by Chenni et al. [2007], taking the wind induced cooling into account is vital in modelling the performance ratio accurately, so this is the method that will be used here, see equation (2.1.5) and figure 2.4. TamizhMani et al. [2003] also showed that the use of additional or a non-linear relation for the climate variables in modelling the performance ratio does not result in a better model for the performance ratio, so I shall make use of the third method.

$$P_R = 1 + \gamma \left(T_{cell} - T_{ref}\right) \tag{2.1.5}$$

where $\gamma = -0.005$ °C^{-1} and the $T_{ref} = 25$ °C is the standard test condition temperature for photovoltaic cells. The cell temperature T_{cell} is modelled by formula (2.1.6).

$$T_{cell} = c_1 + c_2 T + c_3 I + c_4 V \tag{2.1.6}$$

where T is the air temperature around the cell in °C, I is the short-wave downward radiation in W/m^2 and V the wind speed around the cell in m/s. The constants $c_1 - c_4$ have been determined by [TamizhMani et al., 2003] and reaffirmed by [Chenni et al., 2007] to be $c_1 = 4.3$ °C, $c_2 = 0.943$, $c_3 = 0.028$ °C m^2 W^{-1} and $c_4 = -1.528$ °C s m^{-1}.

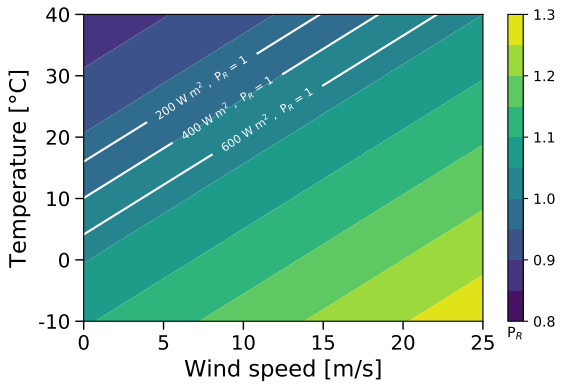

Figure 2.4 – Solar cell performance ratio as a function of temperature and wind speed is shown for a constant value of the incoming radiation ($I = 400$ W/m^2), the plotted lines show the effect of a variable value of the incoming radiation for a constant value of the performance ratio ($P_R = 1$).

2.1.3 Installed capacity

The second piece of the puzzle in modelling the energy production of renewable energy sources is the spatial distribution of the installed capacity for that source. The spatial distributions of installed capacities of on- and offshore wind turbines, rooftop solar panels and utility-scale solar power plants that are used in this study are developed by *Bas van Zuijlen* and *Machteld van den Broek* as part of their research at the Utrecht University Copernicus Institute of Sustainable Development. The distribution of the installed capacity is shown in figure 2.5. The considerations made in developing this projected distribution of installed renewable energy sources are shortly discussed below.

The source of the total installed capacity for each technology is the large scale renewable energy sources scenario from the e-Highway2050 project, see Sanchis [2015]. From this projection the total national installed capacities are used and then downscaled to a subnational level. The downscaling is based on the outcome of the EC-Earth climate model, historical hourly demand data, and geographic land use data. The downscaling method the same as the one used by European Environment Agency [2009].

The total installed capacity in the distribution used is 376.4 GW in onshore wind turbines, 100.6 GW in offshore wind turbines, 119.2 GW in roof-based solar panels and 41.8 GW in utility-scale solar power plant. The ratio between wind and solar energy in this study is therefore 75.5% wind and 24.5% solar based capacity.

The wind turbine hub-heights used in this study are 80 m for onshore wind turbines and 120 m for offshore wind turbines. The choice for these specific values is that current, state-of-the-art wind turbine heights are between 80-100 m for both on- and offshore wind turbines, but it is expected that the height for offshore wind turbines will be less limited by societal considerations [Breton and Moe, 2009], [Kaldellis and Zafirakis, 2011].

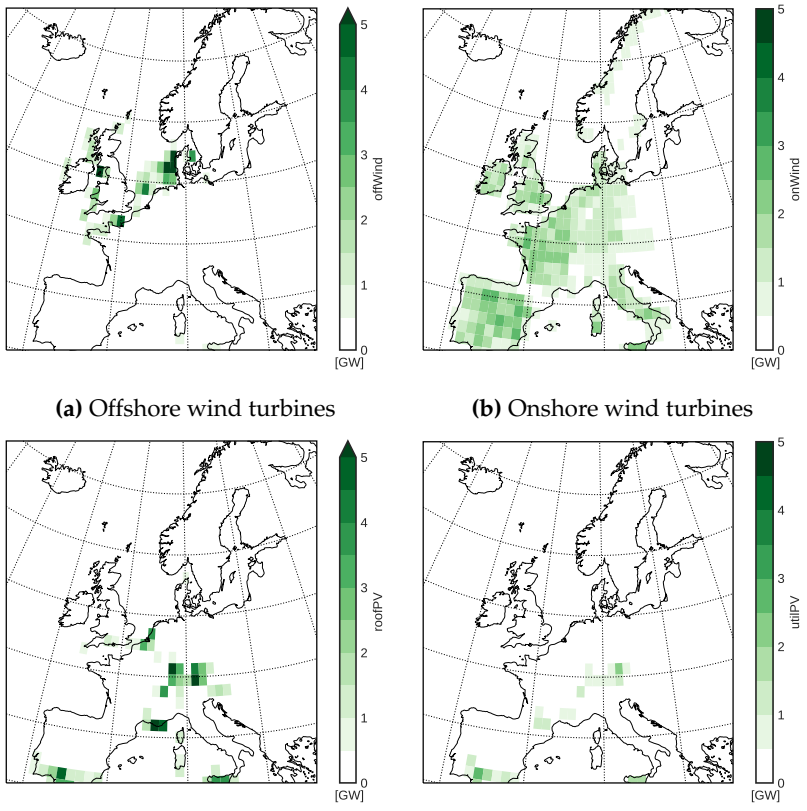

(a) Offshore wind turbines

(b) Onshore wind turbines

(c) Roof based solar panels

(d) Utility-scale solar power plants

Figure 2.5 – Projected distributions of the different renewable energy sources used in this study.

2.1.4 Operational time consideration

The last piece of the puzzle in determining the energy production of a renewable energy source is the operational period of the energy source for each time step in the data used. Even though the model time step is 20 minutes, the output of the simulation is only stored every 24 hours due to storage limitations. As wind turbines can operate throughout the day and night, the operational time used for wind turbines is set at 24 hours [Ravestein et al., 2018]. The story for solar panels is different, they can only be operational during the day and the day length change throughout the year [Forsythe et al., 1995]. Before the day length calculation is explained in more detail, it is important to note that no repair or maintenance time is taken into account in this study.

The number of daylight hours during a single day of the year can be calculated as a function of day of the year and latitude. A model comparison study by Forsythe et al. [1995] determined that the Center for Biosystems Modelling (CBM) day length model is the most accurate. The calculation of this model can be divided into three parts, which are shortly discussed below in equations (2.1.7) to (2.1.9). All trigonometry is done in radians rather than in degrees.

In the first step of the CBM daylight model the revolution angle of the Earth (θ in $^\circ$) is predicted from the day of the year (J, a scalar).

$$\theta = 0.2163108 + 2\tan^{-1}\left\{0.9671396\tan\left(0.00860 \times (J - 186)\right)\right\} \tag{2.1.7}$$

Then the sun's declination angle (ϕ, in degrees), or the angular distance at solar noon between the Sun and the equator, is calculated from the earth's revolution angle.

$$\phi = \sin^{-1}\left\{0.39795\cos(\theta)\right\} \tag{2.1.8}$$

Finally the daylength (D, in hours and including twilight), is calculated using the latitude (L in degrees), the sun's declination angle and the twilight parameter (p in degrees).

$$D = 24[hours] - \frac{24[hours]}{\pi}\cos^{-1}\left\{\frac{\sin\left(\frac{p\pi}{180}\right) + \sin\left(\frac{L\pi}{180}\right)\sin(\phi)}{\cos\left(\frac{L\pi}{180}\right)\cos(\phi)}\right\} \tag{2.1.9}$$

The twilight parameter can be used to tune the day length to adjust for the twilight hours of the day. As solar panels are not operational during these hours, a value of the twilight parameter of $p = 0$ is used here. Modelled day length starts when the sun is completely above the horizon.

2.1.5 The compound energy production impact parameter

In summary, the energy production of wind and solar energy can be determined using equation (2.1.1). For this information on the wind and solar energy potential (section 2.1.1, 2.1.2) from climate model data, see section 2.3. The installed capacity (section 2.1.3) and the operational time (section 2.1.4) are used to obtain their energy production.

The gridded energy production data of each renewable energy source is then aggregated for the whole Western European region considered in this study. The compound energy production is then defined as the sum over the region total energy production of the combined renewable energy sources. Compound energy production is a one-dimensional variable that is only dependent on time and can thus be used as an impact measure [Zscheischler et al., 2018].

2.2 Modelling energy demand

To calculate the energy shortage impact parameter the production of energy and the demand of electricity should be determined. Before we describe how the energy shortage impact parameter is calculated (section 2.2.3), we describe how energy demand is modelled. The production of energy is described in section 2.1.

The societal demand for energy depends, among others, on outside air temperature [Valor et al., 2001]. When it is cold outside, we tend to spend more time indoors to warm up and we are more likely to turn on the (electrical) heating. On the other hand, when it gets really warm outside, we are also more likely to spend time indoors, but then to cool down with the help off air conditioning or a fan. So there is a minimum energy demand at some comfortable temperature and any deviation from that temperature will increase demand, either due to a desire for heating or due to a desire for cooling. This non-linear behaviour makes it difficult to model energy demand in a straightforward manner, see Pardo et al. [2002], Moral-Carcedo and Vicéns-Otero [2005], Bessec and Fouquau [2008], Thornton et al. [2016], Bloomfield [2017] and Staffell and Pfenninger [2018].

However temperature is not the only variable that determines demand. So before we discuss the model for energy demand in section 2.1 it is important to consider what other influences there are on the energy demand, see section 2.2.1. The energy shortage impact parameter that will be used to determine high impact events is explained in section 2.2.3. Figure 2.6 shows a flowchart of how the different data variables are combined in the calculation of the daily energy shortage.

2.2.1 Weather dependent demand

It is important to consider that temperature is not the only property that influences demand. Therefore the main known features that influence energy demand are shortly discussed here. First the very short, sub-daily, and very long time scales are discussed, then the sub-yearly variability in demand due to the rhythm of society. Where needed a short explanation is given on how the influence discussed is filtered out of the demand to better show the influence of weather on energy demand.

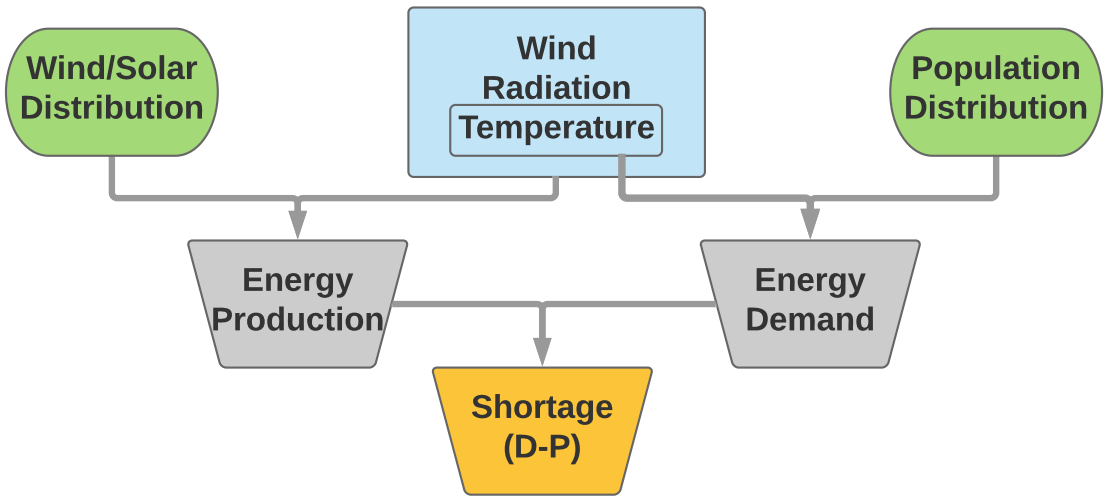

Figure 2.6 – Flowchart of the calculation method for daily energy shortage. In green the spatial distribution and population data, blue shows the climate variables used and in orange the energy shortage is shown.

The very short and very long timescales

On daily timescales the energy demand fluctuations are mostly governed by the clock of society and not by temperature. In this study the total daily energy demand is thus used as it gives a clearer view of the impact of the weather on demand. See chapter 2 of Bloomfield [2017] for a more in-depth discussion on the sub-daily timescale and its aggregation to daily timescales.

On multiyear timescales a non-climatological rising trend in demand can be seen due to the increasing population size, the steady electrification of society and technological improvements leading to more efficient use of electricity, see [Thornton et al., 2016] for an extensive discussion of the long-term trends in energy demand. This multiyear trend is stepwise removed for every year in the demand calibration dataset to better show the influence of temperature on demand.

The rhythm of society

The simple fact that society runs on the same clock is one of the main features in the variability of energy demand on the daily to yearly timescales when daily data is studied. The four most influential of these effects are shortly discussed below and summarized in figure 2.7.

The first effect is the weekly cycle of demand. On Friday, the industry grinds to a halt and people are less likely to work, only to restart on Monday, reducing the daily energy demand in the weekend by 20-40% relative to an average weekday. In figure 2.7 this can be clearly seen by the large difference in the weekend demand, in blue, and the filtered demand, in red. As this effect is very clear and very constant in its timing, the weekend days are filtered out when our energy demand model is calibrated [Moral-Carcedo and Vicéns-Otero, 2005], [Bloomfield, 2017].

The second effect is the industry summer shut-down. Every year at the start of August the industry and construction sector take a four-week break during the peak of summer. This effect is most prominent in the middle of August when week and weekend days are no longer distinguishable in their energy demand, see figure 2.7. As the start of this summer vacation depends on the exact timing of the weekdays near the start and end of August, the whole month of August is filtered out when the energy model is calibrated [Valor et al., 2001].

The third effect is the winter break around New Year. Already a couple of days before the start of Christmas people start to get ready for the celebrations, industry and society starts to slow down. Until the end of the first week of January, energy demand is significantly reduced, see figure 2.7. To filter this effect when calibrating the energy demand model, the arbitrarily chosen start at the 21st of December and end at the 6th of January are used to filter this period. Using a longer period might improve the filtering of this effect, but would also reduce the correct sampling of energy demand during the coldest period of the year [Moral-Carcedo and Vicéns-Otero, 2005].

The fourth effect is caused by the various bank holidays throughout the year, for example see Moral-Carcedo and Vicéns-Otero [2005] for the bank holiday effect in Spain. Bank holidays can be clearly seen as days comparable to a weekend day in figure 2.7. However, bank holidays are not uniform over the region considered in this study and therefore they are kept in the data.

In summary, by filtering out the energy demand changes due to the rhythm of society on the daily, weekly and yearly scale. A clear double seasonal cycle can be seen in the filtered demand of figure 2.7. When this is plotted as a direct function of regional mean temperature, some correlation between temperature and energy demand emerges. However, the non-linear correlation becomes very strong after the population density is used as weighting factor for the regional mean temperature, see figure 2.8. This is because the response of energy demand to weather conditions is caused by where people live [Valor et al., 2001].

2.2.2 The logistic smooth transition regression model for energy demand

The basic reason for the non-linear response of energy demand to population weighted mean temperature (figure 2.8) are the different effects the summer and winter have on cooling and heating habits. In the winter people turn on their heating if the temperature drops below a comfort threshold and in the summer they turn on their air conditioning if it gets too warm, in both cases driving the demand for energy. Generally this non-linearity is captured by using heating

degree days and cooling degree days, see [Bessec and Fouquau, 2008] for an overview and the use of this method. However, the degree day method has some drawbacks, the two most significant of which are listed below. The first drawback is that a single, fixed, arbitrary threshold point is chosen between heating and cooling degree days. These are country specific and are not scalable to the whole region considered [Bessec and Fouquau, 2008]. The second drawback of this method is the use of two societal impact parameters, which makes it ill-suited to study high-impact events. These two drawbacks make the heating and cooling degree day method unfit when the European-wide energy demand is considered.

An alternative method for modelling energy demand was presented by Moral-Carcedo and Vicéns-Otero [2005]. By using a comfort threshold region instead of a threshold point and by smoothing this transition region, they found that the link between temperature and energy demand is more closely matched. The specific method they adopted in their model is the Logistic Smooth Transition Regression (LSTR) method from [Terasvirta, 1994]. They applied this method to the double linear regression of heating and cooling degree days, see equations (2.2.1) and (2.2.2), to obtain their LSTR model. The advantages of this model are that the temperature threshold value is estimated in the fitting of the model rather than being imposed *a priori* and that this model allows for a transition region, rather than a transition point.

The LSTR model is given by equation (2.2.1). The LSTR model shown here is written in such a way that the smoothing function G and the two linear relations can be clearly seen in the model. Mathematically the model is the same as Moral-Carcedo and Vicéns-Otero [2005].

$$E_{filtered\ demand} = [\alpha_1 + \beta_1 T] \times (1 - G) + [\alpha_2 + \beta_2 T] \times G \tag{2.2.1}$$

where α_1 and α_2 are zero degree crossings of the linear functions, β_1 and β_2 are the slopes of the linear functions. The first branch (α_1, β_1) is the heating driven branch of the LSTR model and the second branch (α_2, β_2) is the cooling driven branch of the LSTR model. Where the G is the smooting function $G(T, \gamma, c)$ that is given by:

$$G = (1 + \exp\left[-\gamma(T - c)\right])^{-1} \tag{2.2.2}$$

where c is the inflection point between the two branches and γ is the smooting factor.

LSTR model calibration

The LSTR model developed by Moral-Carcedo and Vicéns-Otero [2005] depends relies on six parameters that are dependent on the situation that the model is applied to. As there is no study

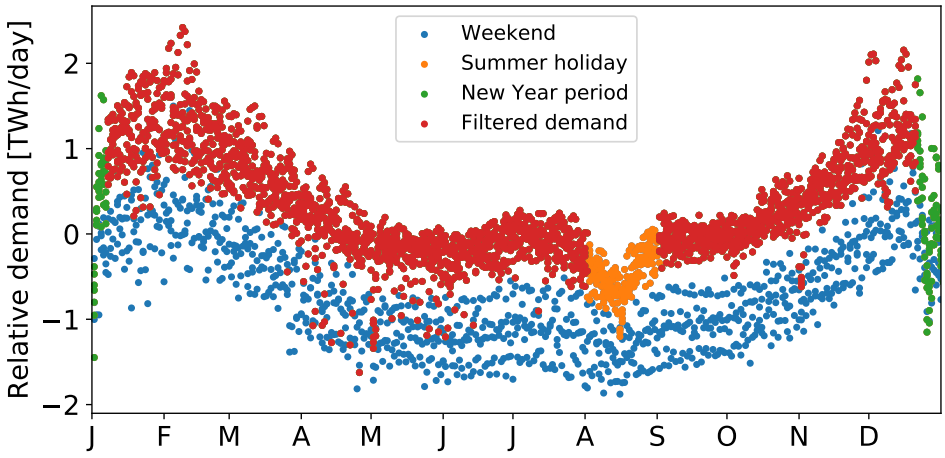

Figure 2.7 – Daily relative regional total energy demand plotted for each day of the year, labelled per month. The demand shown is relative to the yearly mean daily energy demand before the filters were applied. The significant time periods that are filtered out are shown. The European wide energy demand data from 2006-2015 was provided by ENTSO-E.

that applies the LSTR model for energy demand to the whole region under consideration or that uses recent energy demand data, the model needs to be calibrated anew for this. In the next two paragraphs the data used to calibrate the model and the fitting parameter values found will be discussed. The resulting LSTR model can be seen in figure 2.8.

To calibrate the LSTR model, historical hourly demand data for the period 01/01/2006 – 31/12/2015 from the Western European region was provided by European Network of Transmission System Operators for Electricity (ENTSO-E). The data was aggregated to regional daily total demand and filtered as described in section 2.2.1, see also figure 2.7. Then using the Gridded Population of the World (GPWv4) dataset from the Socioeconomic Data and Applications Center (SEDAC) of NASA as weights, the regional average 2 metre temperature was calculated from the ERA-Interim re-analysis dataset.

The LSTR model, as described in section 2.2.2, was then fitted on the filtered demand and weighted temperature average, using a robust least squares fitting method. The method used determined outliers of the data and ignored these points in the fitting procedure, see the dashed lines in figure 2.8 for the outlier boundary. The resulting LSTR model for the western European region then uses the parameters from table 2.1.

The fitting method used is very robust as it ignores outliers, but it has an artificially large uncertainty in the slope of the heating and cooling line due to the automated selection of outliers. As some strong outliers are expected due to the presence of bank holidays in the energy demand data used, this error is treated as artificial and is therefore ignored. In the filtered demand data in figure 2.7 some of the outlier bank holidays can be seen.

2.2.3 The energy shortage impact parameter

In summary, the energy demand can be determined using the LSTR model, equations (2.2.1) and (2.2.2). To calibrate the LSTR model, we use historical demand with the socioeconomic influences filtered out, section 2.2.1. This filtered demand is then coupled to historical temperature data that is weighted by population density, see section 2.2.2.

The projected regional energy demand is then obtained by taking the regional average of the population weighted temperature data from the climate model and using this as input for the

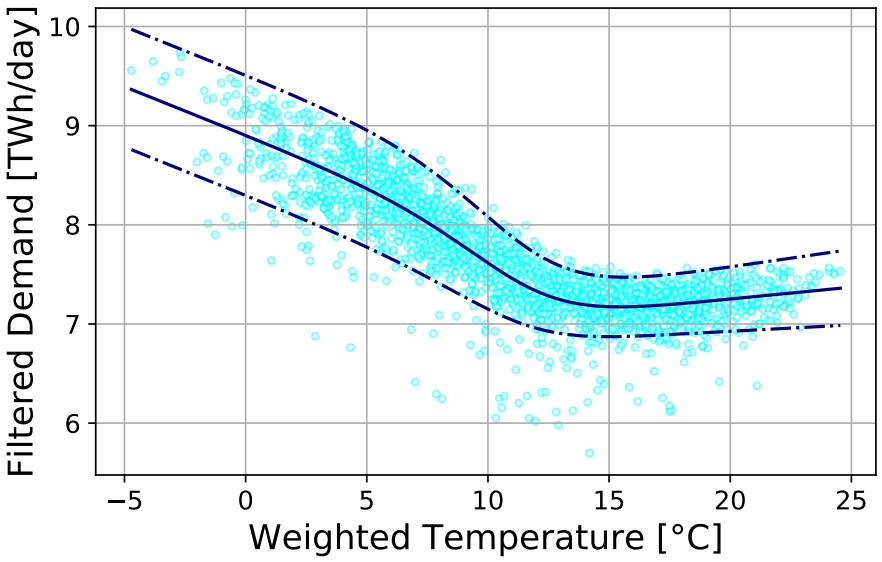

Figure 2.8 – Filtered energy demand is shown as a property of the population weighted temperature in light blue. The solid blue lines indicate the fitted LSTR model function that is used to define energy demand as a function of weighted temperature. The dashed blue lines indicate the boundaries of the points that are used in the fitting procedure, points outside these dashed lines are determined to be outliers by the fitting method.

Table 2.1 – The LSTR model fit values based on the ENTSO-E demand data and the NASA SEDAC global population data as weights for the ERA-interim 2 metre temperature dataset. (*) indicates an artificially high error measure due to the fitting method used, see dashed line in figure 2.8 for the boundary of the points taken into account.

Parameter	*Fit value*	*Uncertainty*	*Unit*
α_1	8.91	$\pm$ 0.61	TWh/day
β_1	-0.10	* $\pm$ 1.15	TWh/day/°C
α_2	6.78	$\pm$ 0.08	TWh/day
β_2	0.02	* $\pm$ 0.12	TWh/day/°C
γ	0.52	$\pm$ 0.02	$°C^{-1}$
c	11.17	$\pm$ 0.52	°C

calibrated LSTR model. In the calculation of the projected regional demand we assume that the population density and the relation between energy demand and temperature are constant. The energy shortage is the difference between the projected regional energy demand and the compound energy production. Energy shortage is a one-dimensional variable that is only dependent on time and can thus be used as an impact measure for societal impact events [Zscheischler et al., 2018].

2.3 Weather & climate simulations data

In this section the climate data used in this study are explained. First, the method for generating the data is explained in section 2.3.1. Then the properties and configuration of the climate models used are explained, in section 2.3.2 for EC-Earth and in section 2.3.3 for HadGEM2-ES. Finally in section 2.3.4 the ERA-Interim reanalysis dataset used to test the robustness of the results is shortly discussed.

The large EC-Earth and HadGEM2-ES climate model ensemble datasets used in this study have been made for the High Impact Weather Events in Eurazia: selected, simulated, storified (HIWAVES3) project. The goal of this project is to develop storylines on extreme climate events with high societal impacts in the European and Asian regions. A special focus of this project lies in large-scale high impact events. This study fits in the HIWAVES3 project as it identifies potential high impact events due to the use of renewable energy and provides the HIWAVES3 project with an analysis dataset on European renewable energy.

2.3.1 The HIWAVES3 time slice experiments

First the basic principle of the HIWAVES3 time slice experiments shall be explained, after this the background of the long climate model runs and the selected climate states that were used are explained in more detail. In figure 2.9 the data selection for the timeslice experiment of the EC-Earth climate model is shown.

The climate data used in this study are the result of the time slice experiments from the HIWAVES3 project. In this project two global climate models were used to generate a large datasets of possible meteorological conditions for a set climate. By using 16 long climate model runs with different initial conditions a range of ocean states can be generated for the same absolute global mean surface temperature (GMST). Periods of 5 year time slices can then be selected, based on their GMST, to represent a certain climate. For each of these selected periods and long climate model runs, 25 members with perturbed initial conditions were then integrated over a 5 year period. By doing this a total of (16 starts $\times$ 25 runs $\times$ 5 years $=$) 2000 years of daily climatological data is generated for each climate time slice that was selected [van der Wiel et al., 2018].

The long climate model runs used are model experiments that cover the period 1860-2100 using the CMIP5 historical and RCP8.5 projected forcings. Due to the use of the same forcing of the climate models, but different initial conditions, different ocean states are generated for similar GMST climate conditions.

The climate states that are used to select the time slices are the *present-day* and the $2°C$ *warming* climate. The *present-day* climate is the time slice in each model for which the modelled absolute GMST is the same as the observed climatological GMST for the period 2011-2015, based on HadCRUT4 [Morice et al., 2012]. The selected period for the EC-Earth climate model is 2035-2039 and for HadGEM2-ES the period selected is 2008-2012. For the $2°C$ *warming* climate the pre-industrial GMST as given by HadCRUT4 is used, to which a $2°$ warming is added. The selected period for the EC-Earth climate model is 2062-2066 and for HadGEM2-ES the period selected is 2036-2040. The period 1850-1899 is used to define the pre-industrial GMST.

2.3.2 EC-Earth ensemble

The large climate model ensemble used to obtain most of the results of this study is EC-Earth. This Earth System Model (ESM) is based on seasonal prediction configuration of the European Centre of Medium Range Weather Forecast (ECWMF) model and is designed by a consortium of 27 international partners from 12 different countries. The version of the model used in this study is EC-Earth V2.3, this version was part of the CMIP5 project and is also used in other international research projects like CRESCENDO, PRIMAVERA and IMPREX.

EC-Earth V2.3 incorporates the Integrated Forecasting System (IFS) for the atmosphere, cycle 31r1 at the T159/N80, or $1.125°$ resolution, with 62 vertical layers is used. The ocean model used in EC-Earth V2.3 is NEMO version 2 with 42 vertical layers on a flexible $1°$ grid that increases to a

1/3° resolution at the equator. The LIM model is used for ice component and the HTessel model is used for the coupling between the land surface and the atmosphere [Hazeleger et al., 2010]. The EC-Earth model is extensively verified on the short and long timescales [Hazeleger et al., 2012].

2.3.3 HadGEM2-ES ensemble

The HadGEM2-ES ensemble is used in this study to verify the quality of the model simulations and to test the robustness of the results found with the EC-Earth climate model because it includes a different atmospheric model. The HadGEM2-ES model incorporates the Met Office Unified Model for the atmosphere, version 6.6.3 at N96 horizontal resolution (1.857° longitude x 1.25° latitude) with 38 vertical layers is used. The ocean model used in the HadGEM2-ES is the same as in EC-Earth V2.3. The TRIFFID model is used for dynamic vegetation and the UKCA model is used for atmospheric chemistry and aerosols in the ESM. For more information on the HadGEM2-ES model used see [Collins et al., 2011] [Alexander and Easterbrook, 2015].

One peculiarity of the HadGEM2-ES dataset is that the wind fields are calculated on a slightly offset grid with respect to the other data fields. The reason for this is that wind is treated as an advection variable and will thus be calculated on the edges of the normal data grid. As the solar panels and wind turbines are needed on the same grid for the analysis, the surface wind speed is interpolated to the grid of the other variables. This will induce an error, but this is considered to be very small as the grids are effectively transposed.

2.3.4 ERA-interim data

The ERA-Interim reanalysis dataset is used in this study to test the robustness of the results. The atmospheric data for the ERA-Interim dataset is produced by a higher spatial resolution and newer version of the atmosphere model used in EC-Earth V2.3. The specific ECWMF IFS model used is cycle 31r2 at the T255, or 0.54°, resolution, with 60 vertical layers. More information on the reanalysis dataset can be found in Dee et al. [2011]. Model output at the aggregated T159 resolution is used in this study for the period 01-01-1979–28-02-2018. Due to the absence of the daily mean surface wind speed in ERA-Interim model output, the 3 hourly mean zonal and mean meridional wind speeds are aggregated to obtain the surface wind speed.

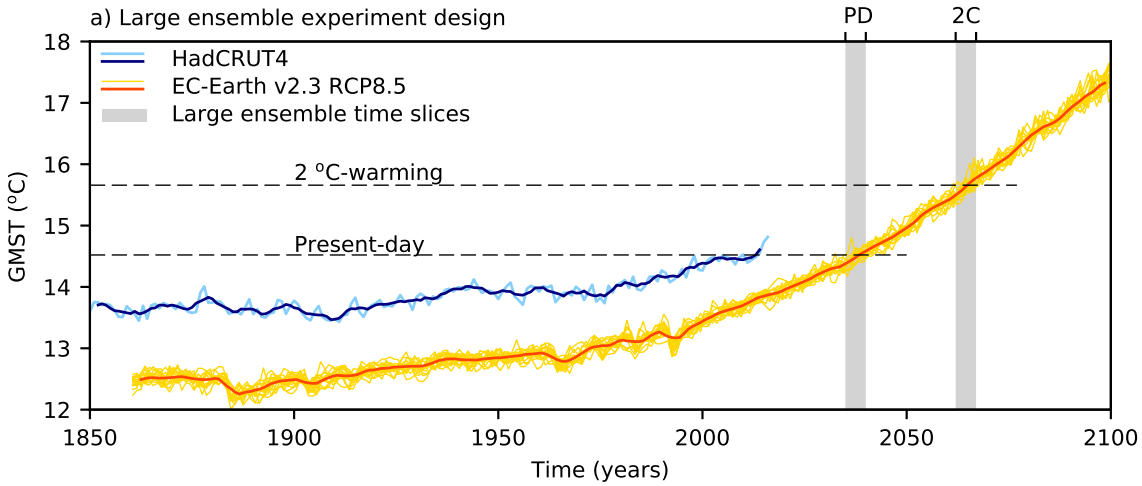

Figure 2.9 – The GMST of the different long climate model runs and HadCRUT4 is shown. The selected climate states (PD and 2C) are plotted in dashed lines and the selected time slice of these climate states is shown in grey. Figure by Karin van der Wiel, reprinted with permission.

2.4 Scope of this research

In this study there are three main limiting factors of the research presented. These limiting factors are the choice of the return time of an extreme event, the durations of prolonged events that are considered and the consideration made for the study region. How each of these factors is limited is shortly explained below. Additionally the definition used for extreme weather will be discussed at the end of this section.

Return time of extreme events

In this study an event is considered a high-impact event if such an event, based on the chosen impact parameter, occurs on average once every ten years. The choice for this 1-in-10 year return time is based on the expert judgement made by researchers at TenneT, the Dutch transmission system operator.

Duration of prolonged events

The durations of high-impact events that are under study here is set to be 1, 7 and 14 days, the choice for this is based on market and societal considerations. As problems with energy production and energy shortage are most severe at the end of the event period, the selection of events is based on the rolling mean on of the impact parameter on the last day. The mean was chosen instead of the energy sum as it would allow for clearer comparison to daily events.

A one-day event could have the highest societal impact, but in that case backup capacity could still be used to limit impacts [Staffell and Rustomji, 2016]. If, however, an event last for a longer period of time the source of fuel for the backup system might run out. Especially if most of the energy demand has to be met with this large scale back-up in the form of biomass, coal or gas power plants. Due to storage limitations the expected timescale for fuel depletion in backup systems is somewhere between 7 and 14 days [Blanco and Faaij, 2018]. This expected maximum timescale for storage and the fact that national transmission system operators make long-term stability estimates 7 days ahead, is the origin of the 1, 7 and 14-day time scales under consideration in this study.

The region under consideration

The study region used here is the Western European region. There are three reasons why this region is considered. The first reason is that the Western European region is considered to have a high share of renewable energy sources around the year 2050. The second reason is that Western European region can be considered as a large interconnected region in which exchange of electricity is possible, a so-called copperplate grid. The third reason is that there are a number of datasets available that have estimations of the projected deployed capacity of renewable energy sources between 2030-2050.

The specific region under consideration in this study encompasses the countries Austria, Belgium, Denmark, France, Germany, Ireland, Italy, Luxembourg, the Netherlands, Norway, Portugal, Spain, Sweden, Switzerland and the United Kingdom. This region will be either referenced by the Western European region or by EU13+2.

Definition of extreme weather

In this study the weather of an event is considered an extreme weather event if the regional mean of the climate variable under consideration occurs on average once every ten years. The regional mean is here defined as the mean of the climate variable over the Western European region. The choice for this definition of extreme weather is for reasonable comparison with high impact parameters. When climate variables are discussed the regional mean value of that climate variable is indicated unless explicitly specified differently.

3 Renewable energy production

To show the meteorological conditions that lead to periods with high societal impact due to the use of compound energy production, four aspects and properties of compound energy production will be discussed here. First, the influence of the different components of the compound energy production impact parameter will be discussed in section 3.1. Then, in section 3.2, the relationship between high impact events and extreme weather will be examined. What the meteorological conditions of the high impact events are, will then be shown in section 3.3. Lastly, the meteorological conditions of prolonged high impact events will be considered in section 3.4.

The method, models and data used for the results that are presented here are discussed in chapter 2.

3.1 Constituents of compound energy production

The constituents of compound energy production are the wind energy and the solar energy sources, as discussed in section 2.1. Before the properties of compound energy production throughout the year are discussed, the properties and features of these two energy sources are examined separately.

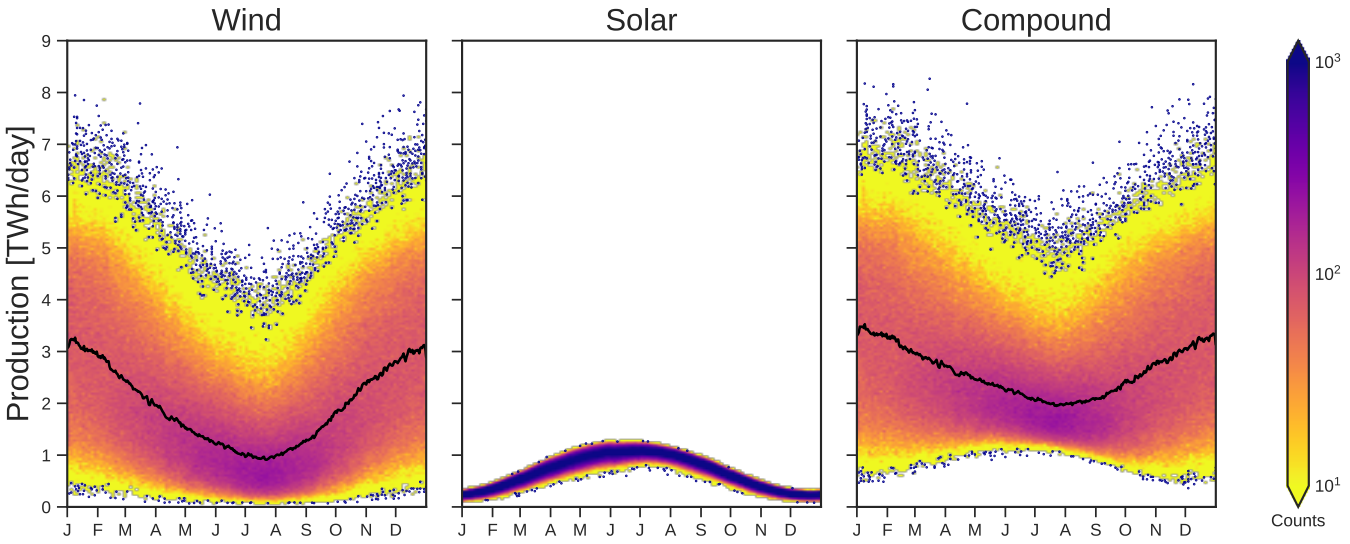

Figure 3.1 – Daily energy production is plotted against the day of the year for wind, solar and compound energy production. The results are plotted as a two-dimensional histogram on a three daily and 50 GWh/day box basis for clarity. The colour of each box indicates the number of events, the blue points indicate a box with only one value, and the black line indicates the daily mean value.

3.1.1 The wind and solar energy production properties

Large differences are observed when the properties of the seasonal distributions of wind and solar energy are compared, as can be seen in the first two panels of figure 3.1. Therefore four most prominent differences in their seasonal distributions are discussed here.

Firstly, the daily variability of wind and solar energy production is radically different, see figure 3.1a and 3.1b. The wind energy production shows a very large daily variability throughout the year, with a winter variability that is almost twice the summer variability. The daily variability of the solar energy production, on the other hand, is very small, especially in the winter or when compared to its seasonal variability.

The second thing to note is the large difference in the daily, seasonal and yearly mean energy production. The yearly mean daily wind energy production (2.08 TWh/day) is triple the yearly mean daily solar energy production (0.66 TWh/day). This is very clear when the lowest daily mean wind energy production (1.23 TWh/day in summer) is compared to the highest daily mean solar energy production (1.00 TWh/day in summer).

The third thing to note is that wind and solar energy production have an opposite and slightly shifted mean seasonal trend. The opposing seasonal trend is very clear as the summer mean wind energy production is significantly lower than the mean winter wind energy production. The mean solar energy production is largest in summer, however. The shift in the maxima of the mean energy production can best be seen in figure 3.1, in the summer period. Here the mean wind energy production has its maxima in the second half of July while the solar energy production has its maxima in the first half of June.

Finally, the season of the highest impact events for wind and solar energy production are opposite. The lowest wind energy production events are observed in the summer, despite the larger daily variability in winter. The lowest solar energy production events are observed in the winter.

3.1.2 Compound energy production properties

When daily wind and solar energy production are combined, into compound energy production, the resulting features are a composite of the properties of the daily wind and daily solar energy production. The three main features of the compound energy production, as seen in figure 3.1c, are briefly examined below.

The variability of the daily compound energy production is like the variability of the wind energy production: very large. In figure 3.1c it appears to be slightly smaller than the variability of wind energy production. However, this is only due to the increased mean energy production in the summer.

The amplitude of the mean daily compound energy production is similar to the amplitude of the solar energy production trend. However, just like the trend in wind energy production, it has the highest amplitude in winter. Where both wind and solar energy production showed a very clear sinusoidal seasonal trend in their daily mean, the daily mean of compound energy production is only by approximation sinusoidal.

The final thing to note is that the season of the highest impacts is the winter. This is mostly due to the large variability compound energy production in the winter, as the winter also has the higher daily mean compound energy production. The most extreme low energy production events are, however, found in the summer, see figure 3.1c.

3.2 High impact compound energy production events

In this section the relation between high impact compound energy production events and extreme meteorology is discussed. High impact and extreme meteorology events are defined as described in respective sections 2.1.5 and 2.4. First the general relation between compound energy production and some meteorological variables is shortly discussed and then the similarities

and differences between high impact events and extreme meteorology is explained for compound energy production.

3.2.1 Relation between compound energy production and meteorological variables

The strongest correlation between compound energy production and a meteorological variable was found with the regional mean wind speed, see figure 3.2a. This correlation is more pronounced if only the summer or winter season is considered (not shown).

As expected, no direct relation is found when the regional mean temperature and compound energy production are considered, see figure 3.3a. This does not change when only one season is selected as there is a very wide range of possible production values for a certain temperature range. Similarly, incoming shortwave radiation and compound energy production show no correlation, see figure 3.3b.

3.2.2 High impact and extreme weather

When the highest impact extremes at a return time of 1-in-10 years are selected, some interesting features of the compound energy production start to become clear. Before this is reviewed in more detail, it is important to again consider that the highest impact events are those events with the lowest compound energy production.

For the highest impact events of compound energy production only one event was also considered an extreme weather event, see figure 3.2b. When the regional mean temperature or incoming solar radiation is considered no high impact event was also an extreme weather event, see figure 3.3a and 3.3b.

3.3 Meteorological condition of high impact events

This section examines the meteorological conditions of the highest impact events due to low compound energy production. To study the meteorological conditions for the highest impact events a

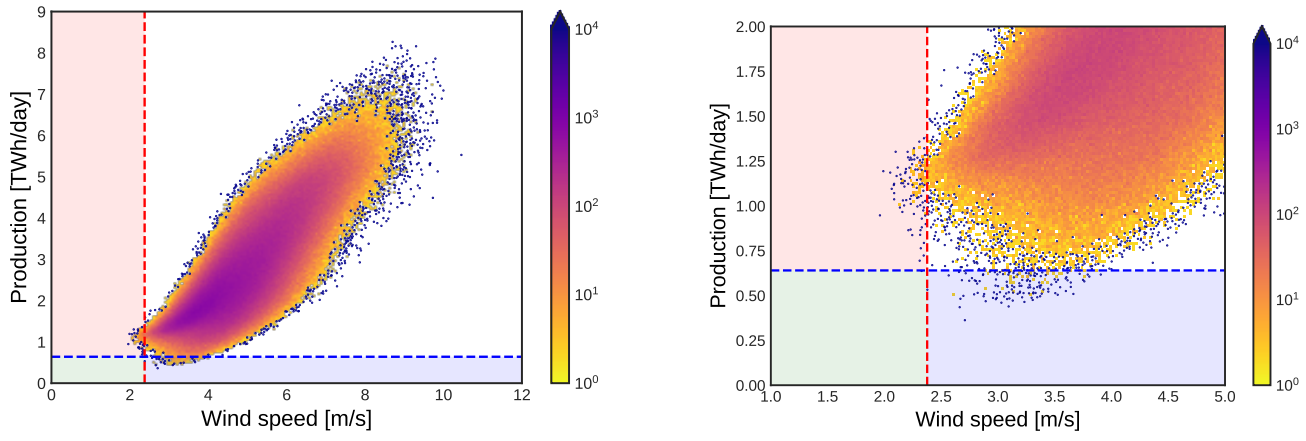

(a) Full scatter plot of wind speed and compound energy production.

(b) Focus of the scatter plot on the extreme event region.

Figure 3.2 – Scatter plot of regional mean wind speed and compound energy production. The colour grading is dictated by a density function of the points, as indicated by the colour bar. Blue points indicate a single point. The red shaded region indicates the lowest regional mean wind speed, extreme weather events. The blue shaded region indicate the high impact events for compound energy production. The green shaded region indicates the region in which a high-impact event is also an extreme weather event.

composite weather map of all 200 1-in-10 year return time high-impact events is made, see figure 3.4.

Based on the composite weather maps as presented in figure 3.4 and on the individual weather maps made for each high impact event, the following three observations can be made.

The first observation is that a very large high pressure system is located over central Europe during these events, see figure 3.4. The exact location is dependent on the specific event, but on average these high-pressure systems are located on the north side of the Alps.

The second thing to note are the low wind speeds during these events. As figure 3.4e shows, the wind speed over most of mainland Europe is below the cut-in wind speed for wind turbines. That the wind speed is low over this region can also be seen from the extended high-pressure system over central Europe and the spread out isobars as this indicates the absence of large scale flow. Wind speeds above the cut-in wind speed for these high-impact events are only observed along the coast of the Iberian Peninsula, around the Baltic Sea and Gulf of Bothnia. In some regions that are outside of the geographical limits of this study significant wind speeds are found, the most promising being the high wind speeds in the surroundings of the Aegean Sea. High wind speeds are also observed over the north-Atlantic and near Iceland.

The third thing to note is that even though all these high impact events are in the winter and daylight hours are very limited, the high pressure system allows for cloudless conditions. So some solar energy production is still observed on the French Mediterranean coast and on the isle of Sicily, as these regions in southern Europe still have a fair amount of daylight hours. In the southern Iberian peninsula also shows solar energy production but a small negative anomaly is observed. Highly limited wind energy production is observed in some locations like Scotland and northern Norway.

When considering these meteorological conditions of high impact events due to low compound energy production, it is important to realize that these events are one-day events that do not show continued extreme low compound energy production over a prolonged period of time. The day before and after the high events show lower than normal wind speeds in the north sea region, though nowhere near as extreme as on the event. At two days from the event this is well within the normal range. Figure 3.4 illustrates this, as it shows composite weather maps of the surface wind speed and wind speed anomaly for the days leading up to and after the high-impact events.

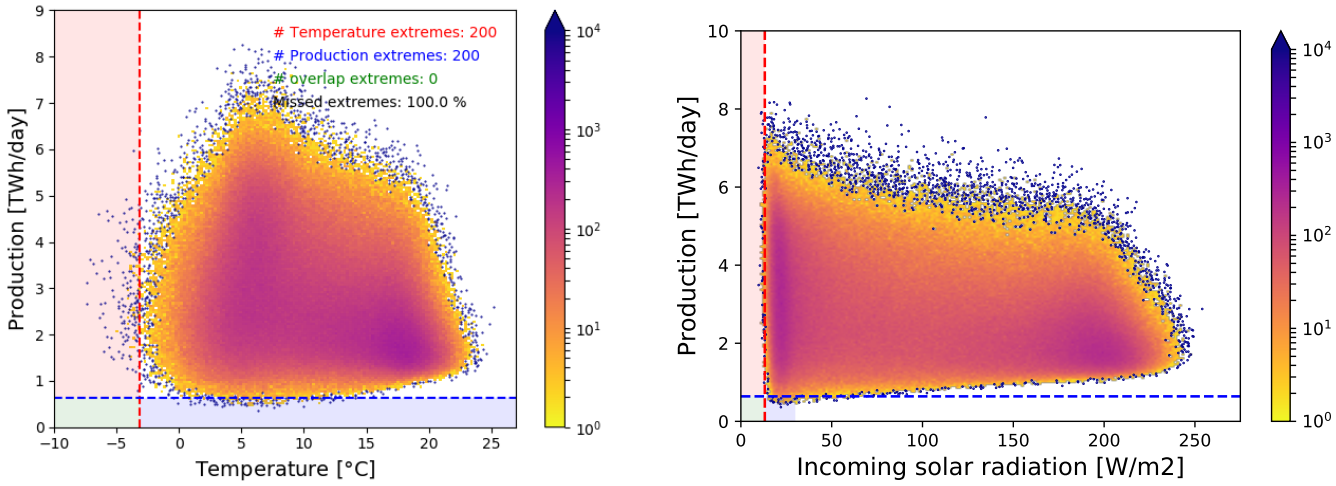

(a) Scatter plot for regional mean temperature

(b) Scatter plot for incoming solar radiation

Figure 3.3 – Scatter plots of a chosen meteorological variable and compound energy production. Colouring as in figure 3.2.

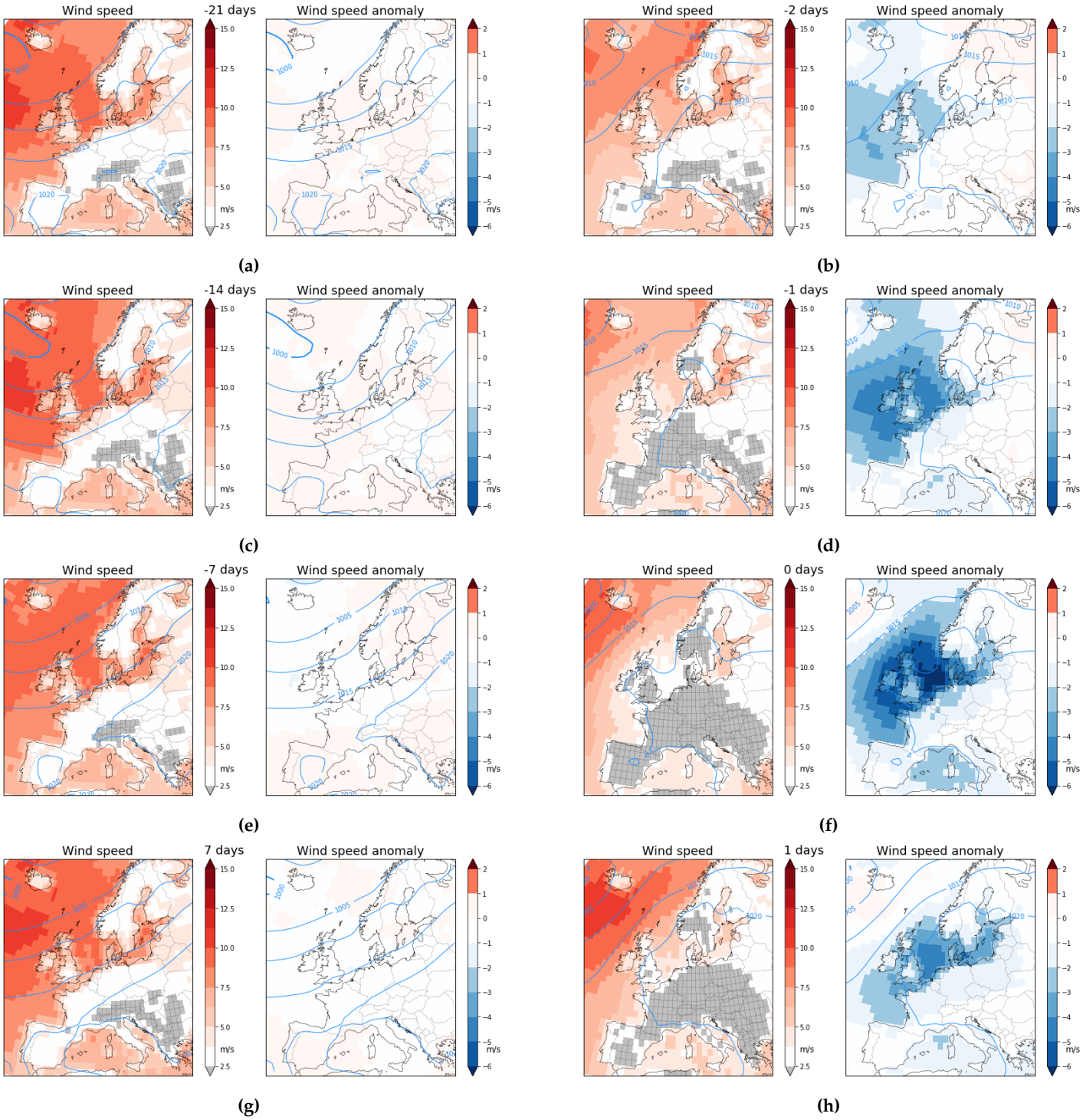

Figure 3.4 – Composite weather maps of the surface wind speed and wind speed anomaly for the days leading up to and after the high-impact events. The left column show composite weather map at (a) three, (c) two and (e) one week ahead and (g) one week after the event. The right column shows the weather map at (b) two and (d) one day ahead of the event, (f) on the day of the event and (h) the day after the event. In blue the isobars are shown surface pressure [hPa]. The background colour shows the gridded values of a selected variable based on the given colour scale.

3.4 Influence of event duration

As was shown in section 3.3 and figure 3.4 the daily high impact events due to low compound energy production are mainly one-day events in a reasonably normal compound energy production period, see also figure 3.6a for compound energy production for the days leading up to the event. When longer event durations are considered this no longer holds, as the days leading up to the event also show low compound energy production, see figure 3.6b and 3.6c. When longer event durations are considered, the selection of the high-impact events needs to be looked at again to make sure the right high-impact events are selected, because the daily variability and mean have changed for the different seasons.

When studying figure 3.5, the first observation that can be made is that the season of the highest 14-day impacts shifts from the winter to the late summer and autumn compared to the highest one-day highest impacts, see figure 3.5 a and c. When the highest 7 day impacts are considered this shift in the season of the extremes can partially be observed, but there are some extremes that occur in the winter months.

The shift in the season of the highest impact events can also be shown when the co-occurrence of 1-day and 14-day events is considered. For instance, there are 2 events that are both a high-impact event on a daily scale and a high impact event on a 7 day scale, but there is no overlap between the daily high-impact events and the 14-day high-impact events.

A different story holds when the relation between the highest societal impact and extreme weather events is studied. For the relation between low compound energy production and low mean wind speed there is only one event (0.5% of the high-impact events) that is considered both an extreme weather event and a hig- impact event on a one-day scale. While, on the other hand, there are 4 and 16 events (2% and 8% of the selected high impact events) that are both classed as an extreme weather and a high impact event for the respective 7 and 14-day event period. For other meteorological variables no overlapping events were found.

In figure 3.7 the composite weather map is plotted for the highest impact events on a 1, 7 and 14-day scale. In Scandinavia warmer than normal temperatures are observed for the prolonged 7-day events. For a 14-day prolonged event the atmospheric state is characterized by a band of high pressure stretching from the centre of the North Atlantic, over England to the Baltic states. With this band of high pressure, higher anomalously warm temperatures are observed in Scandinavia.

That the 7 and 14 day prolonged events are characterized by an earlier onset of the high pressure system and the wind draught that accompanies that is shown in figure 3.6. From figure 3.8 it can be observed that the prolonged 14 day high impact events have a high pressure system that travels over the high pressure band, indicating that these prolonged high impact events are not completly static.

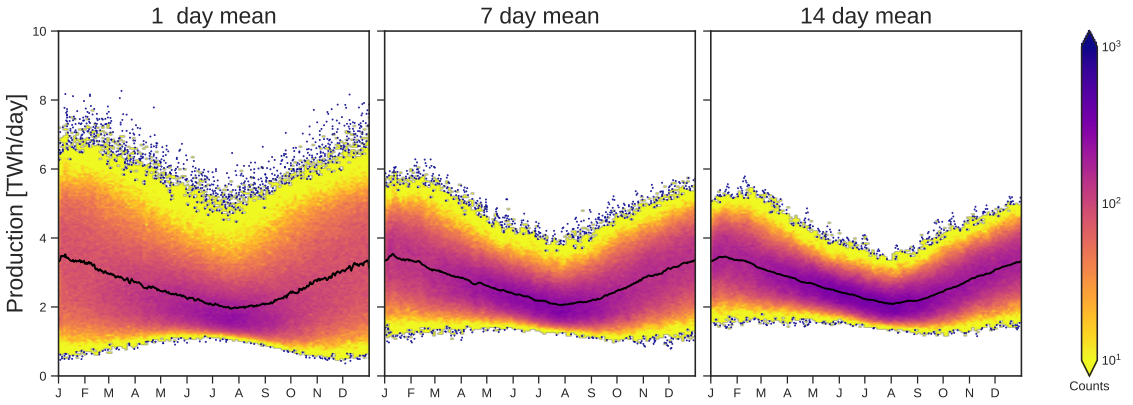

Figure 3.5 – Compound energy production is shown throughout the year for the different periods under consideration. Colouring as in figure 3.1.

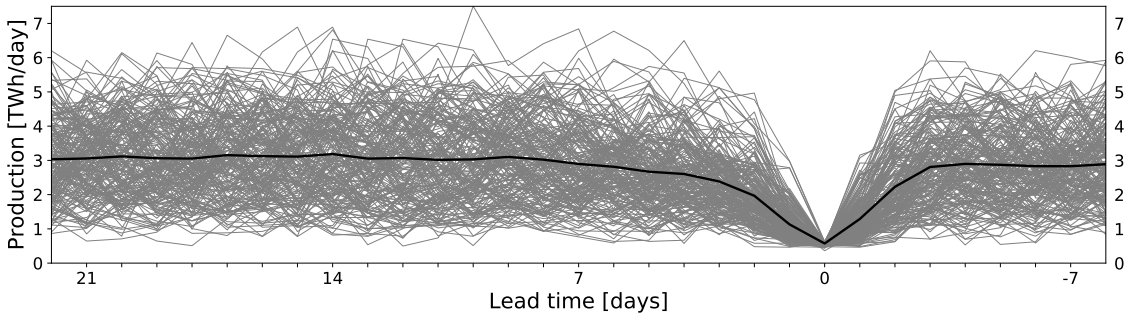

(a) 1 day period

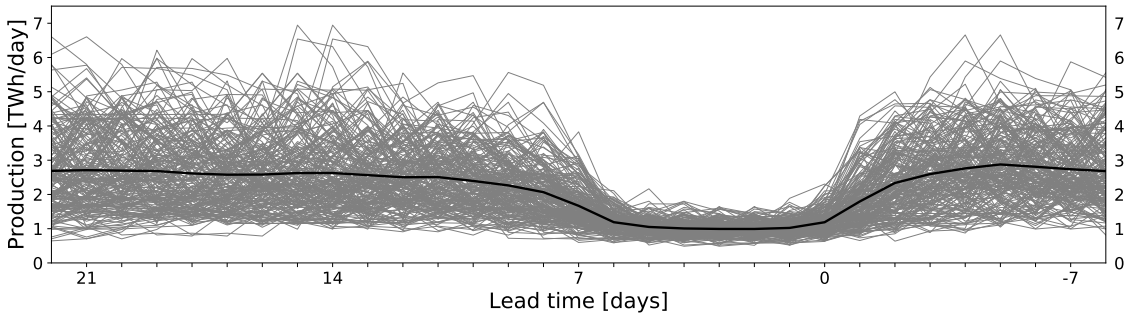

(b) 7-day period

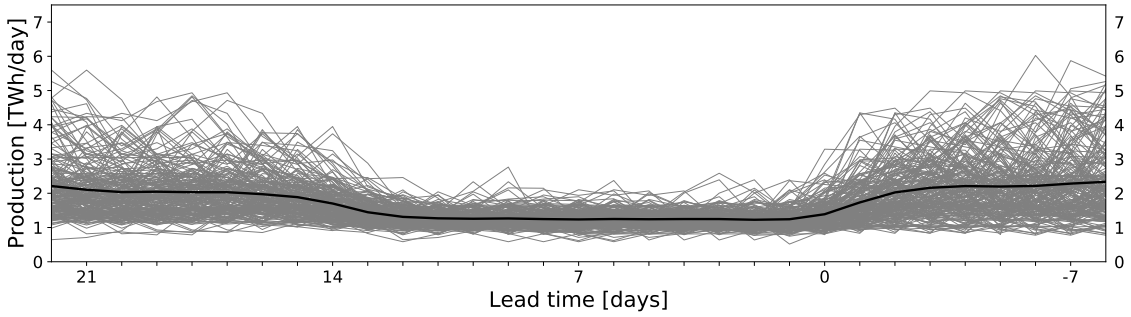

(c) 14-day period

Figure 3.6 – Spaghetti plots of daily compound energy production leading up to different prolonged event length are shown in grey. The black line indicates the mean compound energy production for each day leading up to a high impact event.

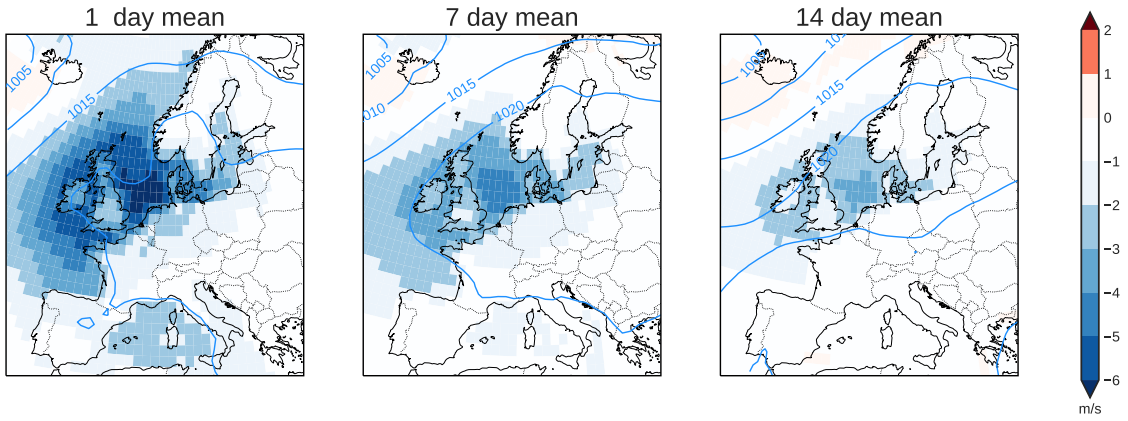

(a) Surface wind speed anomaly from climatology

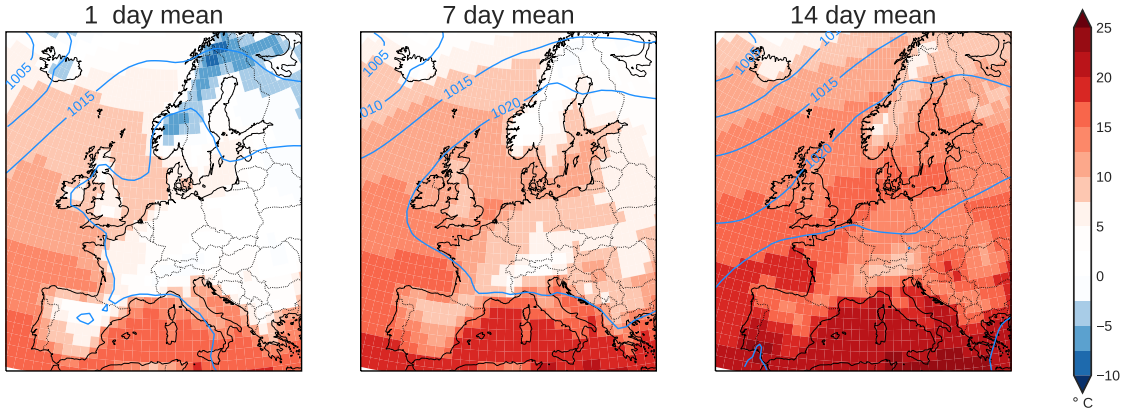

(b) Daily mean 2 metre temperature

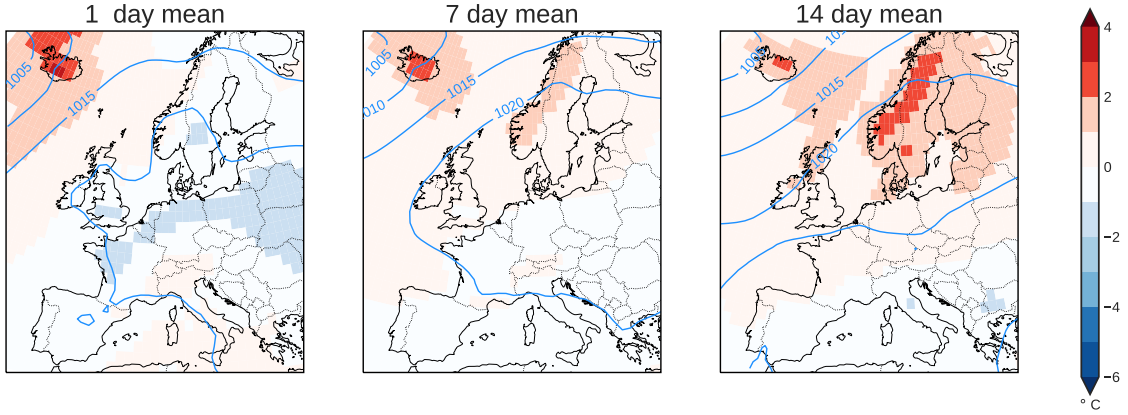

(c) Daily mean temperature anomaly from climatology

Figure 3.7 – Weather maps for a chosen meteorological variable for the highest impact events on a 1, 7 and 14-day time scale, based on the lowest compound energy production. Colouring as in figure 3.4.

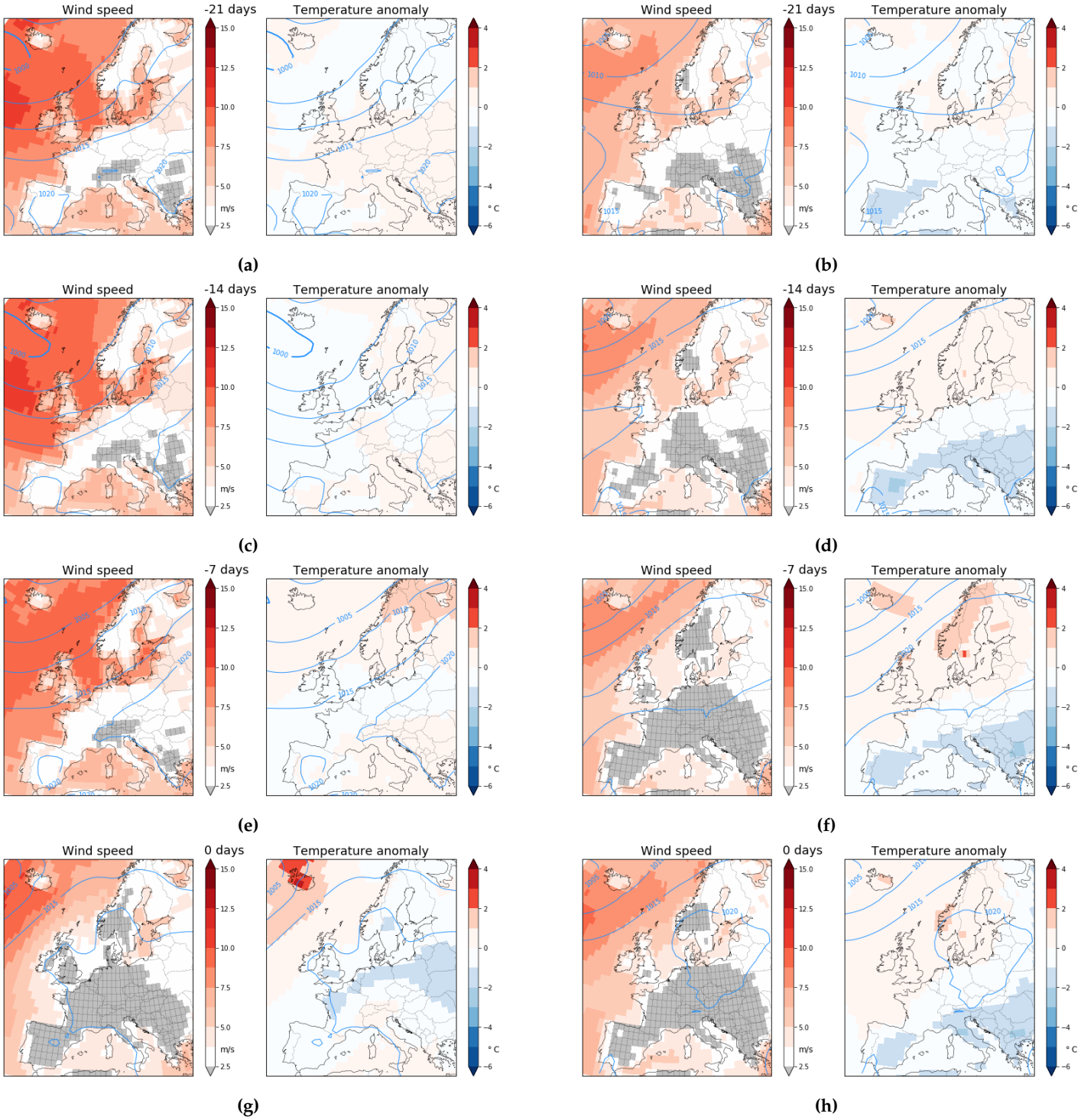

Figure 3.8 – Composite weathermaps of the surface wind speed and temperature anomaly for the days leading up to the lowest compound energy production impact events. On the left the weather before a 1 day high impact event is shown, on the right the weather before a 14 day high impact event is shown. Coloring as figure 3.4

4 Energy shortage

In this chapter the research results for the energy shortage impact parameter will be discussed. Energy shortage is considered here as the difference between projected demand and compound energy production, as defined in chapter 2. The highest societal impacts due to energy shortage are those events that have the highest energy shortage. To show the meteorological conditions that lead to periods with the highest societal impact, four aspects or properties of energy shortage will be discussed here. First the relation between compound energy production, energy demand and energy shortage will be discussed in section 4.1. The selection of the highest impact events and the relation of these events with extreme weather will be deliberated in section 4.2 and their meteorological conditions will be revealed in section 4.3. The influence of the duration of the extreme event on the meteorological conditions will then be considered in section 4.4.

4.1 Constituents of renewable energy shortage

The constituents of energy shortage are compound energy production and energy demand, see figure 4.1. As the properties of compound energy shortage have been discussed in detail in section 3.1, only the properties of energy demand will be discussed here. How the two constituents of energy shortage interact will also be discussed, at the end of this section.

4.1.1 Properties and features of energy demand

When the second panel of figure 4.1 is reviewed, two features of the weather dependent daily energy demand are important to consider. For clarity the two-dimensional histogram for demand is also plotted separately in figure 4.2. It is important to consider that the energy demand that is used here is free of any societal factors like weekends and holidays.

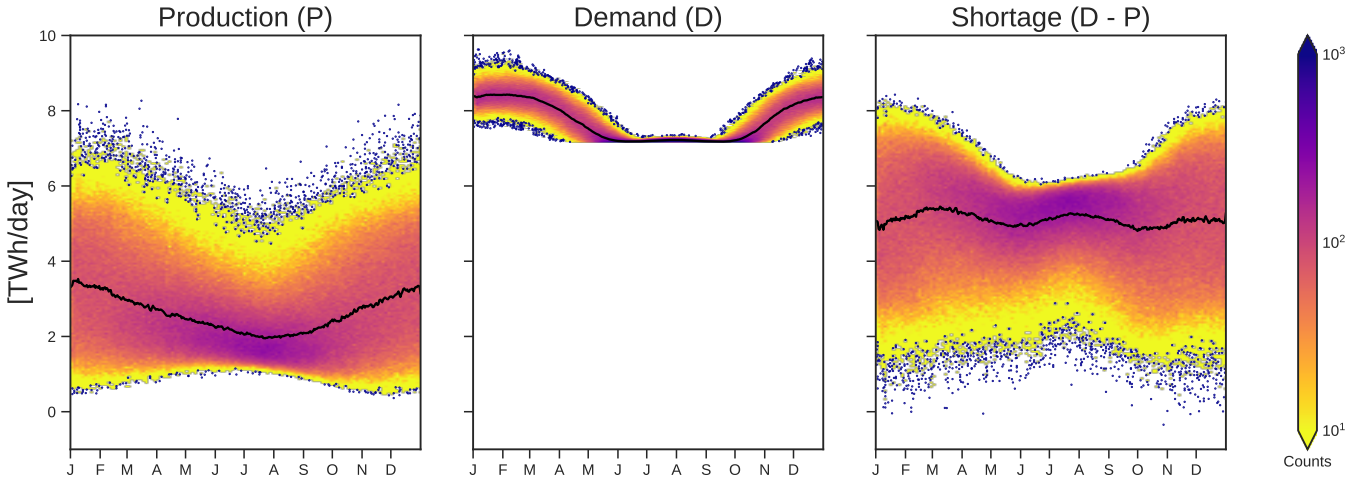

Figure 4.1 – Composition of energy shortage is shown throughout the year as 2D histogram. Colouring as in figure 3.1

The first feature is that there is a strong seasonal component in the mean daily energy demand. The mean daily energy demand is largest in the winter, lower mean energy demand is observed in the summer. However, the lowest mean daily energy demand is not observed in the middle of summer, but in June and September. The same holds for the amplitude of the variability, the largest variability is observed in the winter and the lowest in the months June and September. This can be attributed to the large dependency of energy demand on temperature in the winter months, as shown in figure 2.8.

The second observed feature is that the magnitude of the variability on a seasonal scale is three times smaller than the magnitude of the variability throughout the year of compound energy production. The daily variability of energy demand is found to be 18% around the mean from the start of November until the end of March. In the summer period from mid June to mid September this is only 4%.

4.1.2 Properties of shortage

When daily compound energy production and energy demand are combined into energy shortage, the resulting features are a composite of the properties of these two parts. The three main features of the compound energy production, as seen in figure 4.1 c, are shortly examined below.

The first observation is that energy shortage has the largest variability in its daily values in winter. The large variability of the energy shortage impact parameters is governed by the variability of compound energy production as the variability of energy demand is limited. The variability in energy shortage is observed to be largest in winter and smallest in summer.

The second observation is that the daily mean energy shortage is relatively constant throughout the seasons, but the highest energy shortage events are seen in winter. This is due to the larger variability of energy shortage around the mean in winter compared to summer.

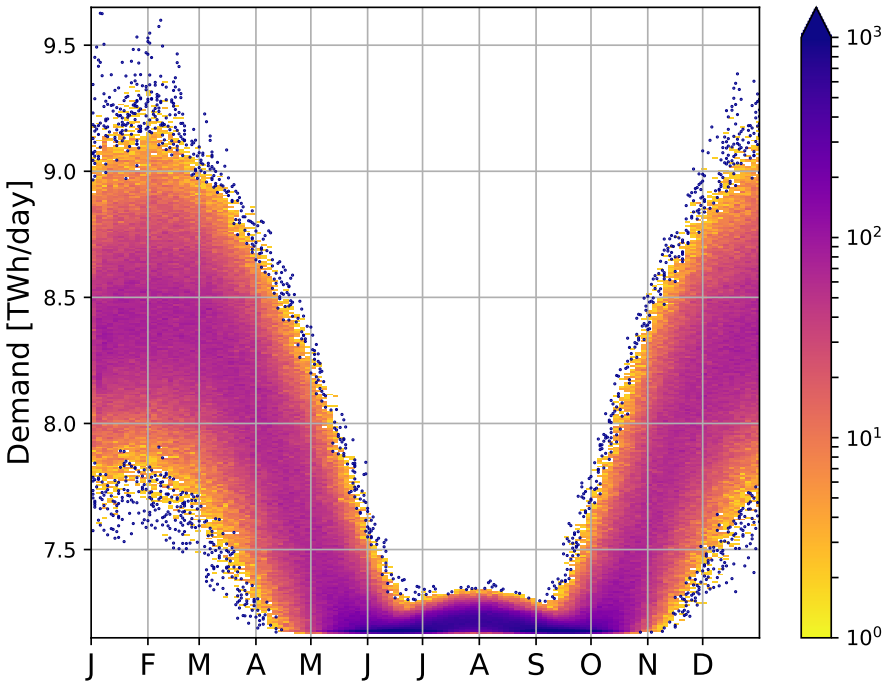

Figure 4.2 – Energy demand is shown throughout the year as a 2D histogram. Colouring as in figure 3.1

4.2 High-impact shortage events

When the highest impact extremes are studied, some interesting features of the meteorological conditions for the highest energy shortage events start to become clear. As before, in section 3.2, the events are selected based on the return time of 1-in-10 years events.

Of all these extreme events 2% was also considered to be an extreme low-temperature event, see figure 4.4a. For both regional mean wind speed and incoming solar radiation, no high-impact event was also an extreme weather event, see figure 4.4b for the first, the latter is not shown.

When the high-impact events of low compound energy production and energy shortage are compared, significant overlap is found between the two high-impact parameters for 13.5% of the high-impact events, see figure 4.4

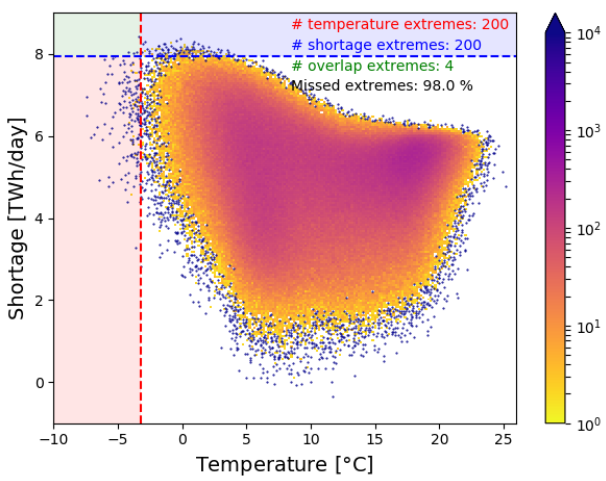

(a) Scatter plot of temperature and energy shortage.

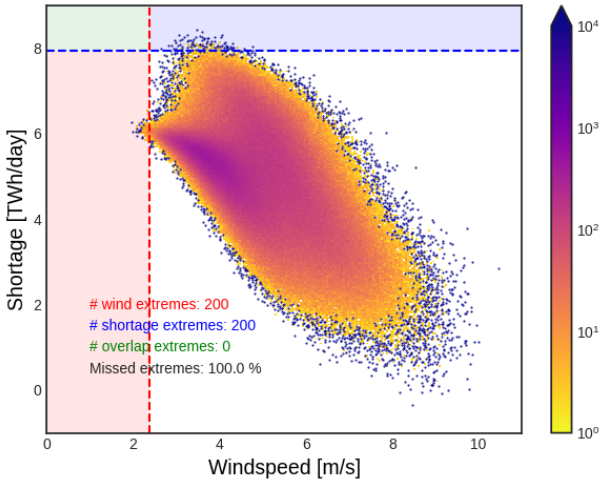

(b) Scatter plot of wind and energy shortage.

Figure 4.3 – Scatter plots of energy shortage as a function of regional mean temperature or regional mean wind speed. Colouring as in figure 3.2.

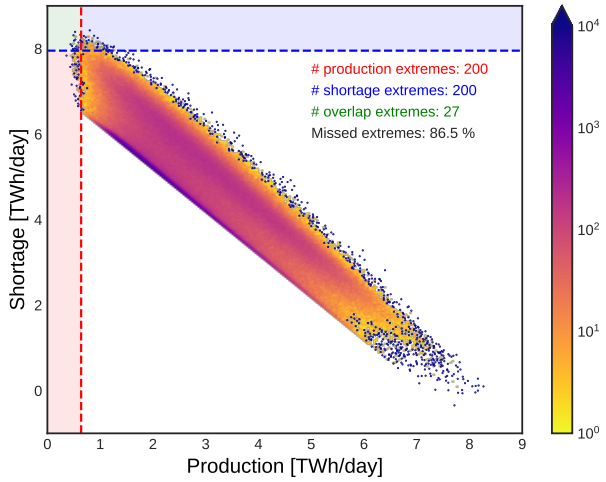

(a) Full scatter plot the impact parameters

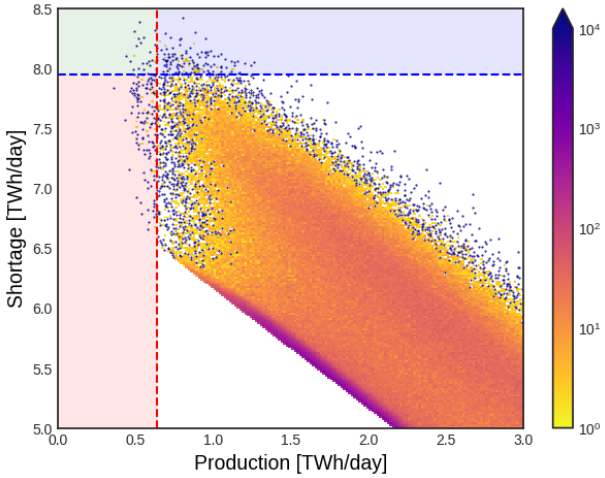

(b) The overlap region of combined high impact

Figure 4.4 – Scatter plot of production and shortage. Colouring as in figure 3.2.

4.3 Meteorological conditions for extreme shortage

This section examines the meteorological conditions of the highest impact events due to high energy shortage. As in section 3.3, a composite weather map is made of all 200 events with a 1-in-10 year return time based on the energy shortage impact parameter.

Based on the composite weather map series as presented in figure 4.6 and 3.4h, the first observation that can be made is that the weather patterns for the high-impact events due to high energy shortage are very similar to the high-impact events due to low compound energy production. They are high-pressure system over Europe leading to low wind speed conditions. There are two distinct differences that between the two impact parameters, however.

The first difference is that the high-impact events due to energy shortage are accompanied by anomalous cold conditions in Central Europe, while the lowest compound energy production events take place under normal temperature conditions, see figure 4.5. Not only is this temperature anomaly present in the highest energy shortage events, as shown in figure 4.6, it is also already present in the days leading up to the event. The presence of these lower than normal temperatures indicates that temperature is the main driver in the creation of these high-impact events.

The second difference between the meteorological conditions for the different impact parameters is that the centre of the high-pressure system that drives these energy shortage events is located further towards the north-west. Furthermore, the extent of the high-pressure system is smaller and less spread out to the south-east.

When considering these meteorological conditions of high-impact events due to high energy shortage, it is important to realize that these events are much more spread out than the low compound energy production events. Even at a week in advance the temperature anomaly is already seen, albeit three times smaller than during the high impact event days, see figure 4.6. That these colder than normal temperatures already appear a week in advance can be seen in figure 4.8a by the steadily increasing daily shortage of energy leading up to the actual event.

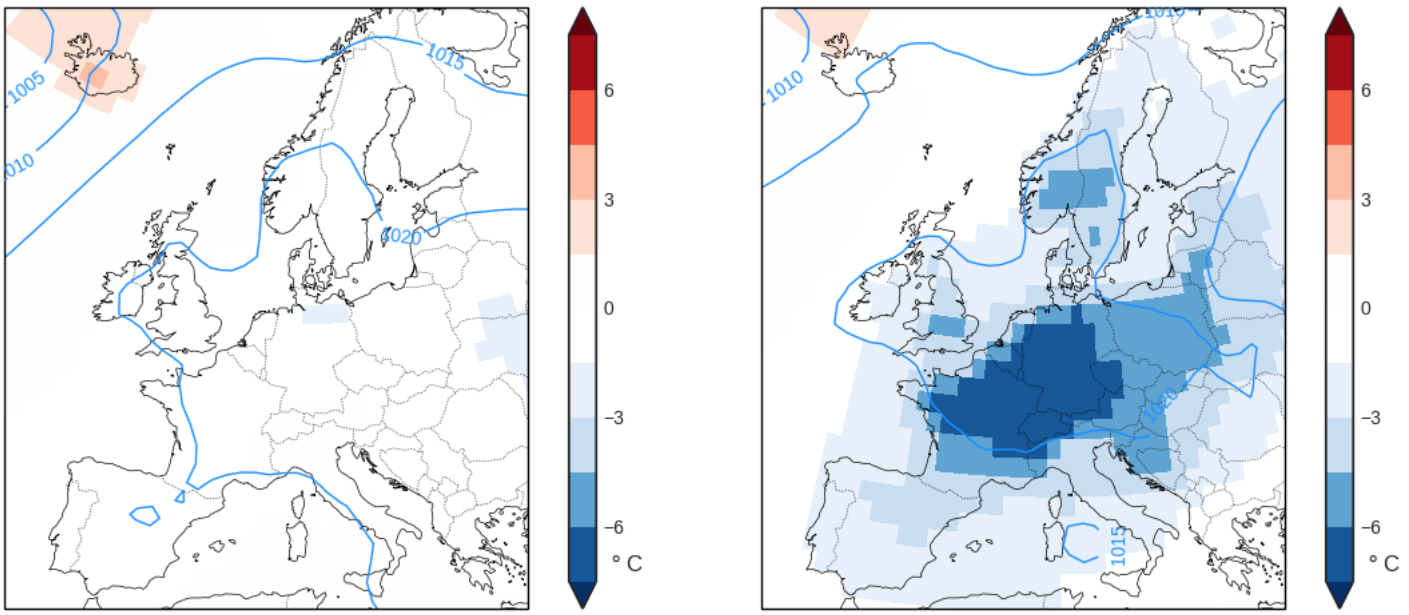

(a) Temperature anomaly for the lowest compound energy production

(b) Temperature anomaly for the highest energy shortage events

Figure 4.5 – Composite weather maps for temperature anomaly of the highest impact events for both impact measures' high-impact events. Colouring as in figure 3.4h.

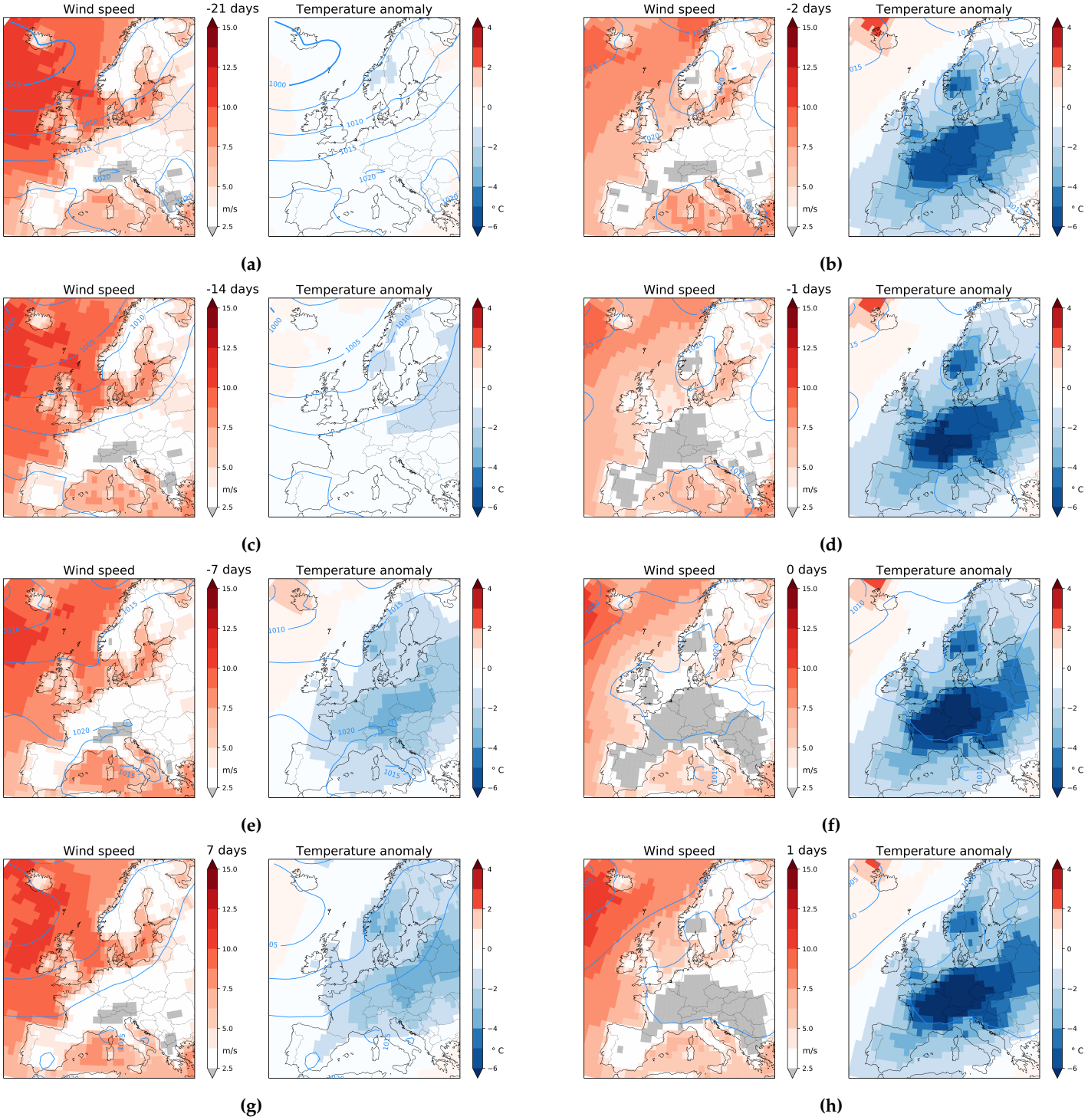

Figure 4.6 – Composite weather maps of the surface wind speed and temperature anomaly for the days leading up to and after the high-impact events. The left column shows composite weather map at (a) three, (c) two and (e) one week ahead and (g) one week after the event. The right column shows the weather map at (b) two and (d) one day ahead of the event, (f) on the day of the event and (h) the day after the event. Colouring as in figure 3.4h.

4.4 Influence of event duration

At the end of section 4.3 it was already indicated that the first signs of high energy shortage can already be seen at a one-week lead time, this can also be seen in figure 4.8a. When longer event durations are considered, this early signal in the days leading up to the event is also seen, see figure 3.6b and 3.6c. As in section 3.4 the selection of the high impact events needs to be repeated in order to determine the right high impact events.

In figure 4.7, the energy shortage for different event durations is shown. The first feature is the reduced variability of the prolonged high-impact events observed throughout the year. This reduction is most severe in winter where the variability goes from 60% of the mean on a daily time scale to 28% of the mean on a 14-day time scale. In summer this variability goes from 16% to 12% of the mean. While the variability of energy shortage is suppressed on longer time scales, no change in the daily mean energy shortage is found. Combining this with the relatively stronger variability in winter, the highest high-impact events for energy shortage are still found in the winter on a 7 and 14-day time scale, see figure 4.5.

When the relation between the highest societal impact and extreme weather events is studied, a reduction of variability is found on 7 and 14-day time scale, but the shape of the relation is similar for the 1, 7 and 14-day events. The overlap between extreme low temperature events and the highest societal impact increases when longer time periods are considered, from 2% for a 1-day event to 4.5% or 8% for a 7 or 14-day event. As expected, no overlap between extreme low incoming solar radiation and extreme low wind speed is found on longer time scales. The overlap in the selected events with high impact due to low compound energy production is drastically reduced when longer time periods are concerned. Where this overlap was 13.5% on a 1-day time scale, 10.5% is still found to overlap on a 7 day time scale, but no overlap is found at the 14-day time scale. When the longer time periods are compared with each other, it is found that of the 1 day highest energy shortage events 13.5% is also 7-day high impact event and 6% of the 1-day events is also 14-day high impact event.

Figure 4.9b shows the temperature anomaly throughout Europe and a clear cold anomaly is observed on a 1, 7 and 14-day time scale. While the magnitude of the cold anomaly is reduced for prolonged events, the spatial distribution of the anomaly is constant when different time scales are considered. This is different when it is compared to figure 4.9a, where the temperature anomaly for compound energy production is plotted. For the highest impact events due to compound energy production, the temperature anomaly observed is not significant and the spatial distribution of the signal of the anomaly is not constant when longer time scales are considered.

Figure 4.9d shows the wind speed anomaly throughout Europe, showing that a negative wind speed anomaly can be observed over the North Sea and the United Kingdom. This wind speed anomaly is very similar to the wind speed anomaly found for the highest impact events for compound energy production, see figure 4.9c, and it shows a similar decrease when prolonged events are considered. There are two minor differences, however. The first difference is that on the longer time scales the wind speed anomaly of the highest energy shortage events is further westward. The second is that for prolonged events a positive wind speed anomaly is found over the Adriatic and Aegean Sea.

Based on the composite weather map series as shown in figure 4.10 for the 1 and 14-day highest impact events, two observations can shed some light on the origin of the weather leading to these high-impact events. The first observation that can be made is that the cold anomaly enters the region from the East over a period of some days before reaching central Europe, where the coldest anomalies are then found. This is similar for both the 1-day and the prolonged 14-day events, although the 14-day prolonged events show the coldest anomalies at 7 days prior to the defined event date. The second observation that can be made for a 14-day prolonged event is that in most of Europe the wind speed is above the cut-in wind speed of wind turbines, thus indicating that energy production is still possible throughout the region.

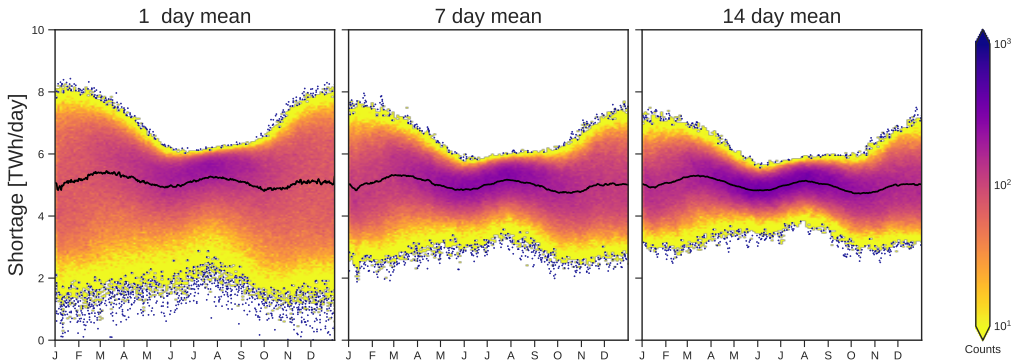

Figure 4.7 – Energy shortage is shown throughout the year in a 2D histogram for different durations of prolonged events. Colouring as in figure 3.1.

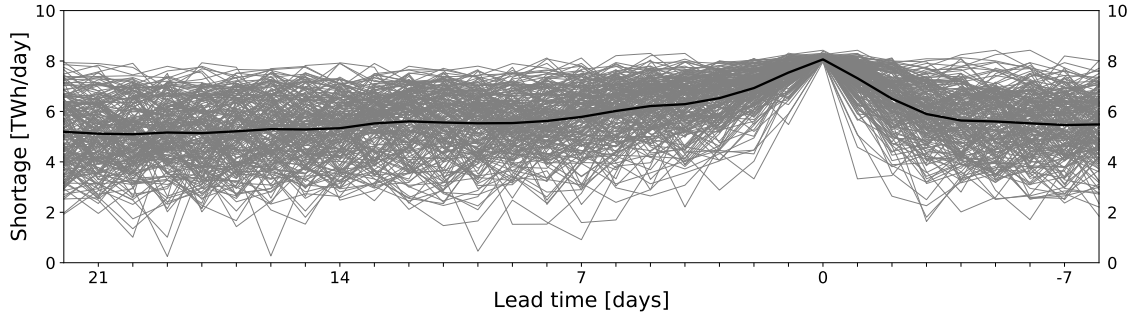

(a)

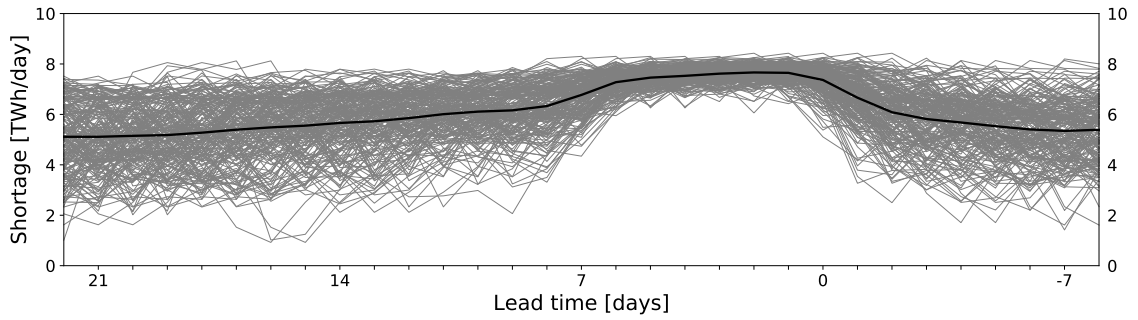

(b)

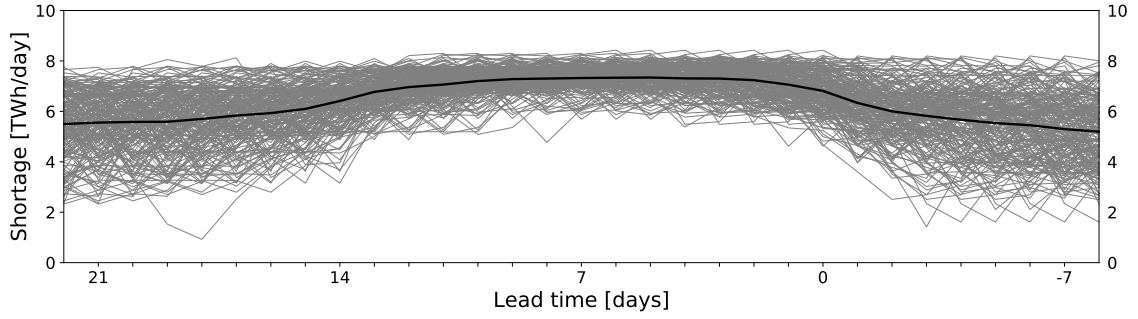

(c)

Figure 4.8 – Spaghetti plots of daily energy shortage leading up to different prolonged event lengths are shown in grey. The black line indicates the mean value for each day leading up to a high impact event.

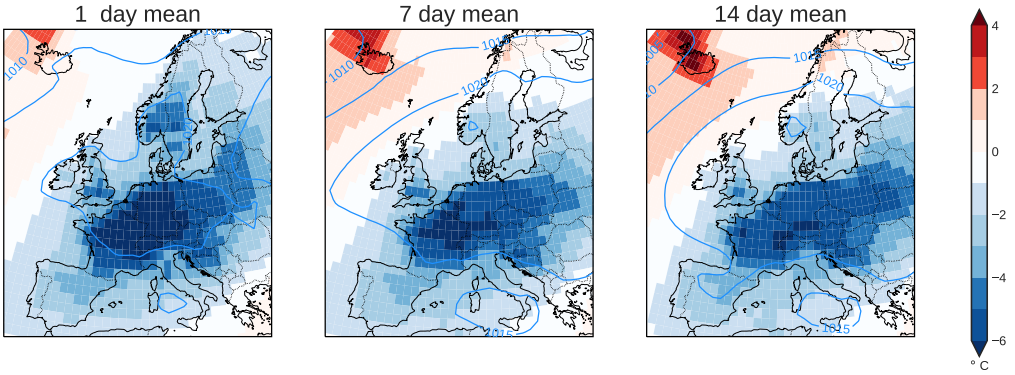

(a) Daily mean temperature anomaly from climatology, for high-impact energy shortage events

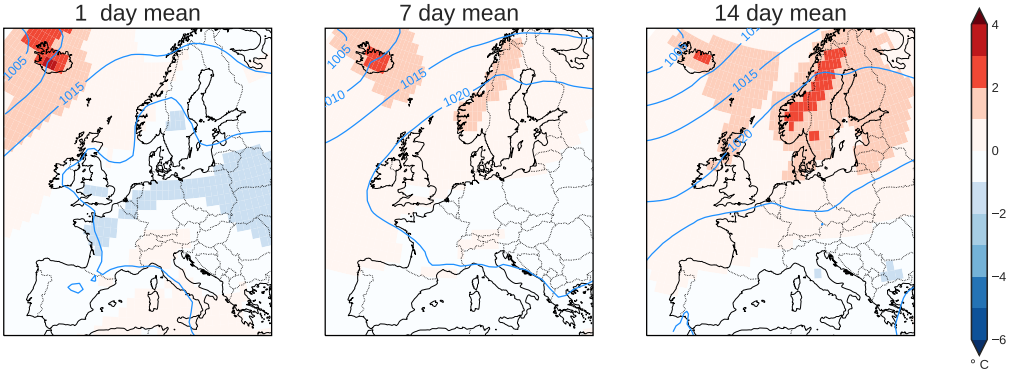

(b) Daily mean temperature anomaly from climatology, for high-impact compound energy production events

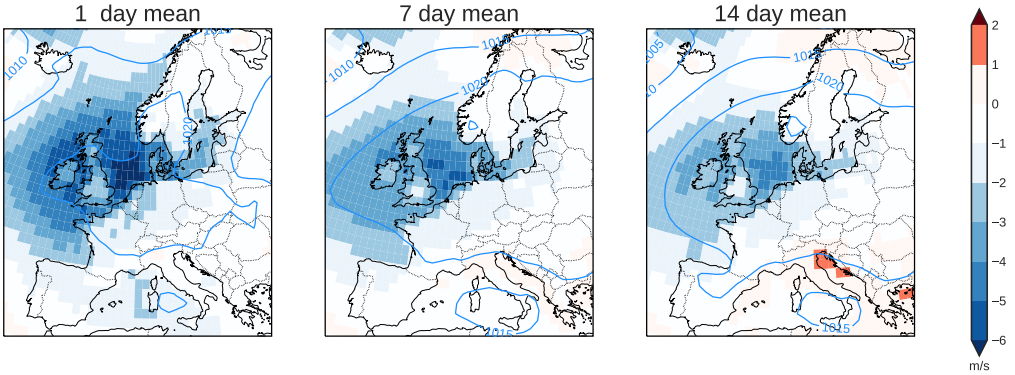

(c) Surface wind speed anomaly from climatology, for high-impact energy shortage events

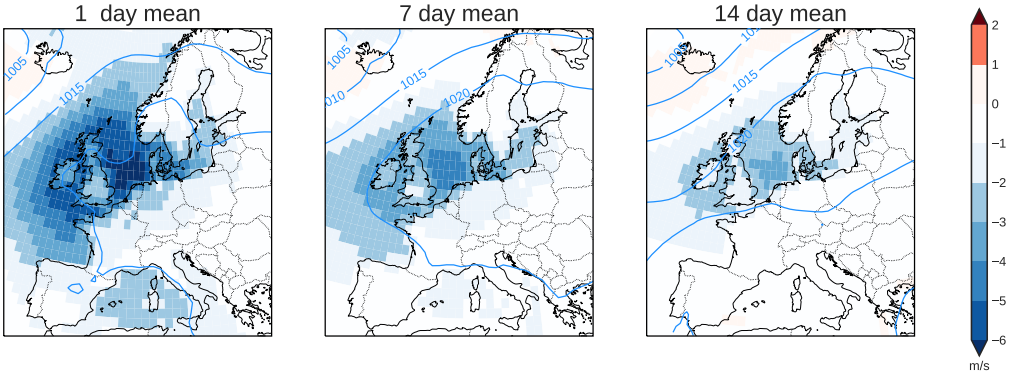

(d) Surface wind speed anomaly from climatology, for high-impact compound energy production events

Figure 4.9 – Weather maps for a chosen meteorological variable for the highest impact events on a 1, 7 and 14-day time scale. Figure (a) and (c) are based on the highest energy shortage events. Figure (b) and (d) are based on the lowest compound energy production events. Colouring as in figure 3.4.

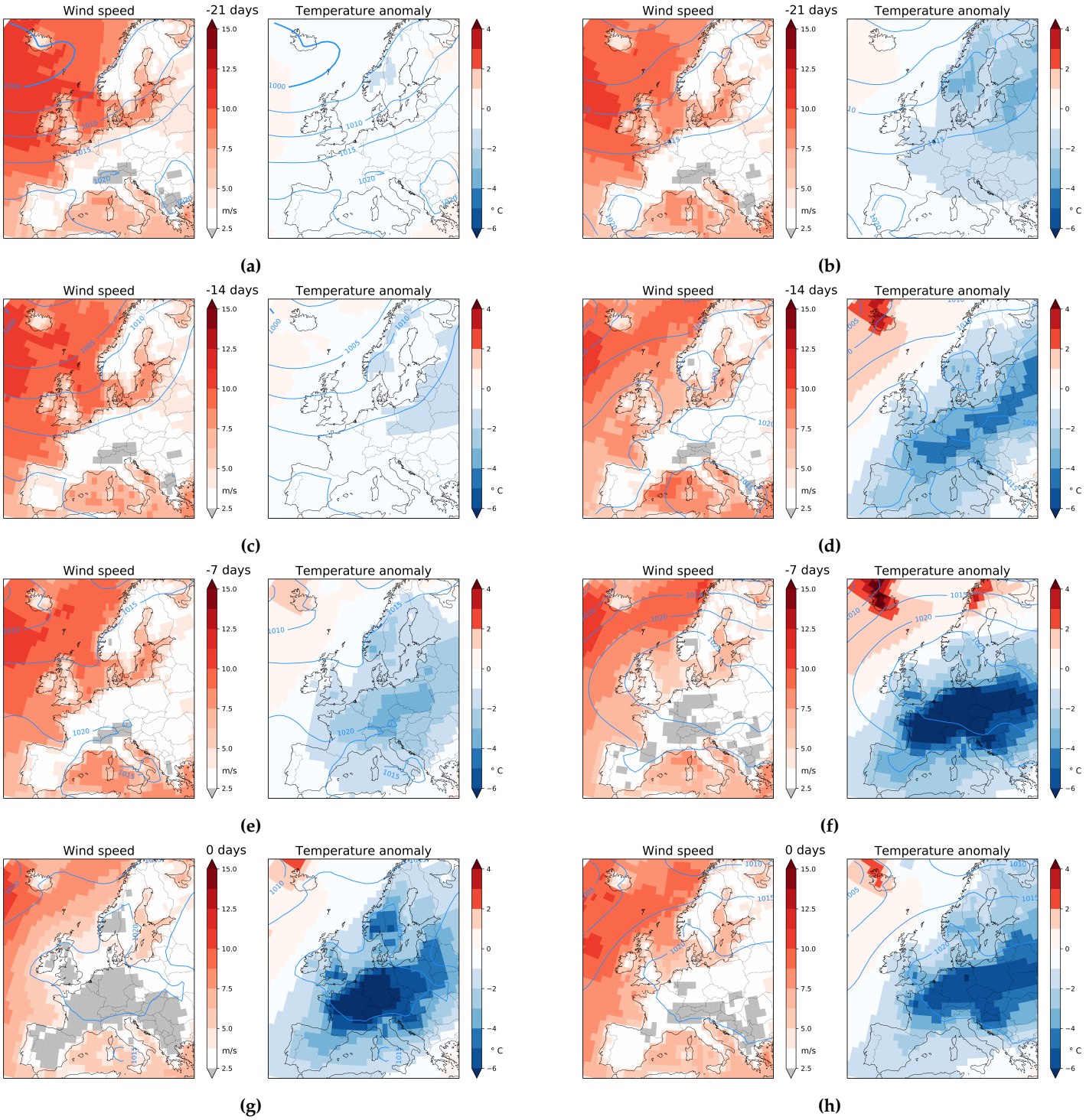

Figure 4.10 – Composite weather maps of the surface wind speed and temperature anomaly for the days leading up to the highest energy shortage impact events. On the left the weather before a 1-day high impact event is shown, on the right the weather before a 14-day high impact event is shown. Colouring as figure 3.4

5 Robustness of results

In this chapter the initial results of the robustness testing of the data used is presented here. The main goal of this chapter is to test how realistic the results are for the method and models used. Innitially the study here was supposed to be extensive, but limitations in time have forced this chapter to be more preliminary.

In section 5.1 the results obtained are compared to the results obtained when the same modelling and analysis method was used on the ERA-Interim data set. Section 5.2 will do the same, but then for the second HIWAVES3 dataset made with the Earth System Model HadGEM2-ES. The dependency of the results on the distribution used and the effects of climate change are then discussed in sections 5.3 and 5.4.

5.1 Comparison with ERAinterim

In testing the robustness of the results obtained in this study, it is vital that a connection to the real world application of the found results is made. The dataset used for that purpose in this study is the ERA-Interim reanalysis dataset. The properties of this dataset are described in section 2.3.4.

To validate the data an initial comparison is made with the available data of ERA-Interim. In figures 5.4a and 5.4c strong similarities in overall shape are seen in the histogram of daily energy production from solar panels and wind turbines.

For solar energy production the location of the low energy peak is the same for both datasets, but the shape of the high end energy production is slightly different. In the EC-Earth data the wind energy produced shows a steeper increase at low energy productions then the ERA-Interim data. The high energy prodcution tail for EC-Earth is also flatter then for ERA-Interim, which continues to higher values then the EC-Earth data.

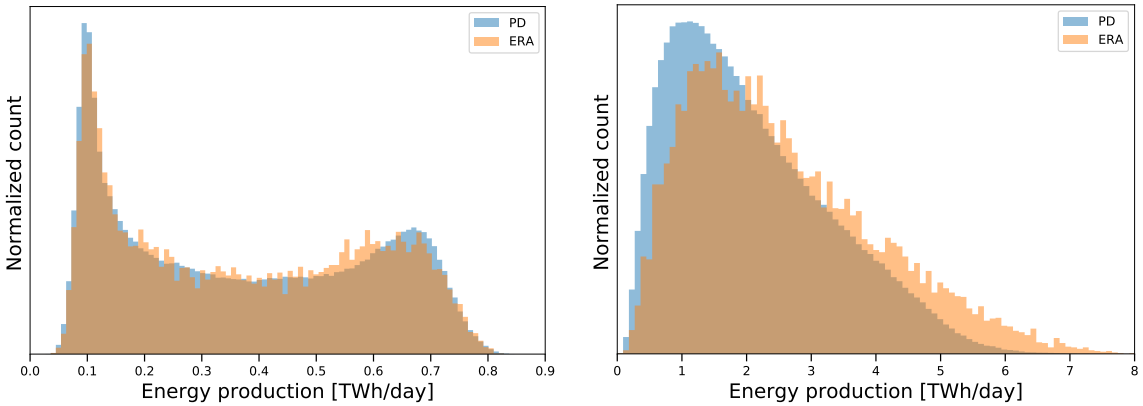

(a) Histogram of daily solar energy production

(b) Histogram of daily wind energy production

Figure 5.1 – Histograms of the daily energy production of solar panels 5.4a and wind turbines 5.4c. Data for the ERA-Interim dataset is shown in orange, in blue the EC-Earth dataset is shown. The count of the number of events for a certain energy production bin width is normalized to allow for comparison between the two climate models used.

In figure 5.2 the two dimensional histogram of daily energy production for the present day EC-Earth and the ERA-Interim dataset is shown. Qualitatively the same behavior can be observed in both the datasets. However when the monthly variability is compared in the form of the percentiles of the data observed some differences are observed, see figure 5.3.

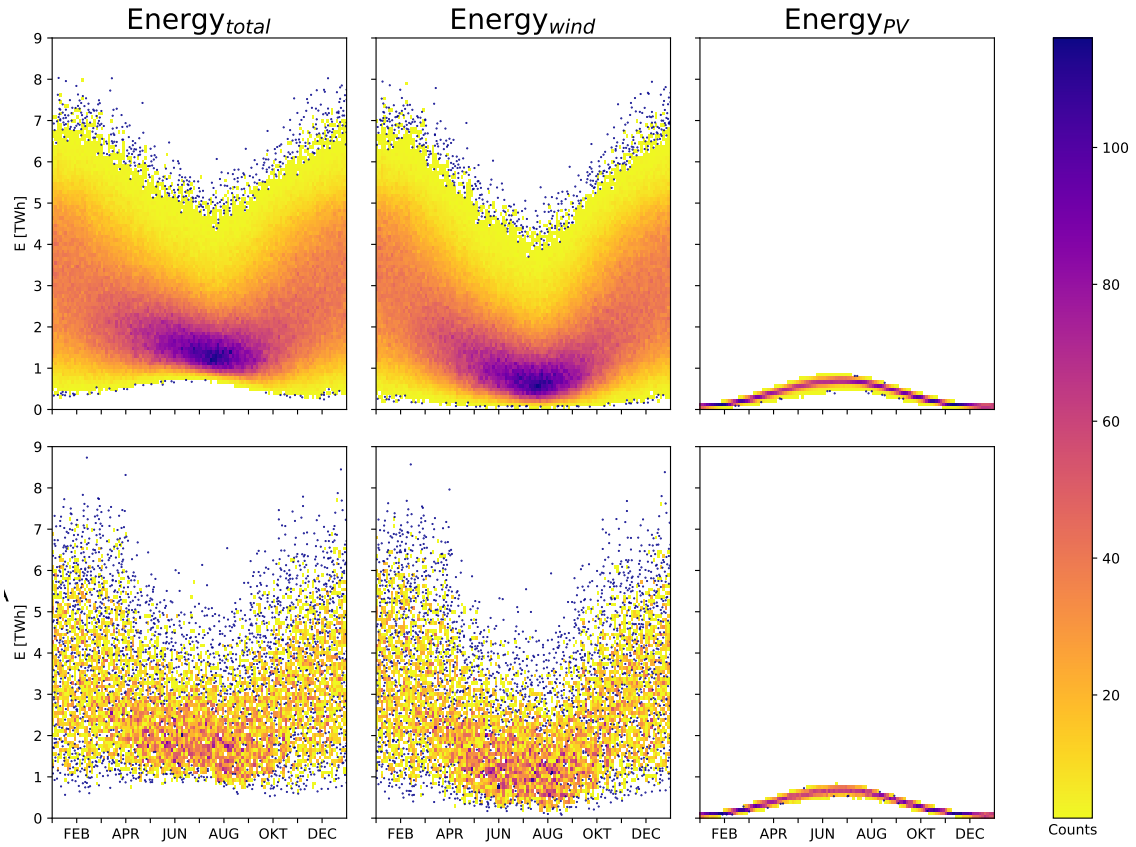

Figure 5.2 – Two dimensional histogram as a function of region wide daily energy production and the day of the year. The top row shows the results for the EC-Earth dataset. The bottom row show the data for ERA-Interim. The color of the bins is scaled by a factor of roughly 52 so that the 2000 years of EC-Earth data is colored as a 38 year dataset like ERA-Interim. Further coloring as in figure 3.1.

As can be seen from figure 5.4, the regional difference in energy production is are largest during the summer season and smaller for the winter period. In general the regional differences in compound energy productin is very small. In some specific region a large signal is found.

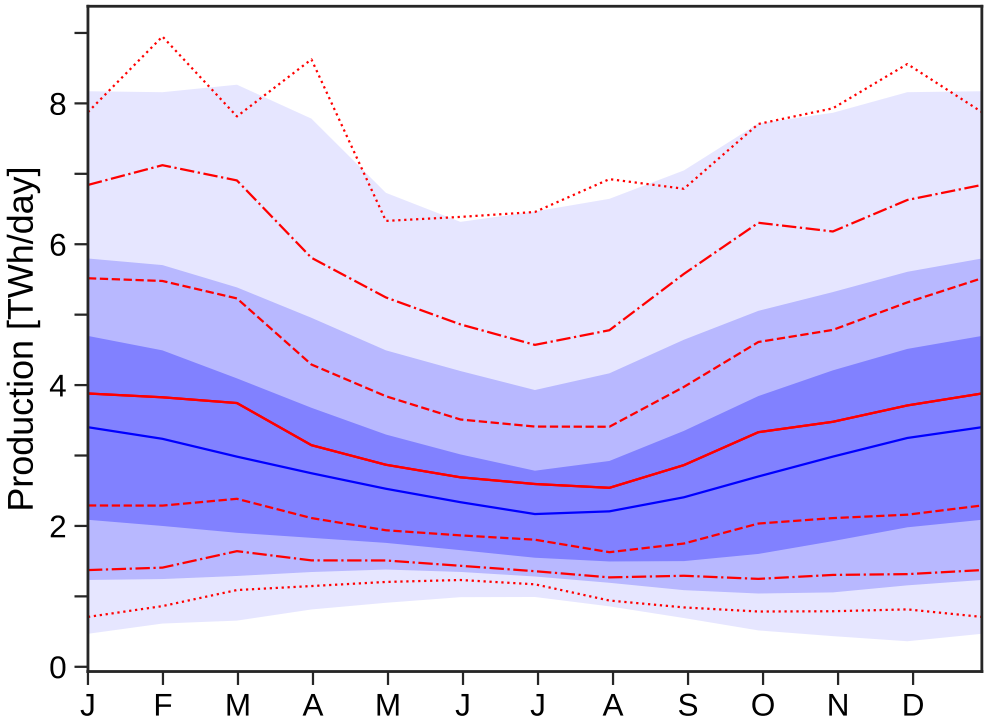

Figure 5.3 – The monthly percentiles of the data are shown for ERA-Interim dataset, red lines. The EC-Earth dataset is given by the blue shaded regions.

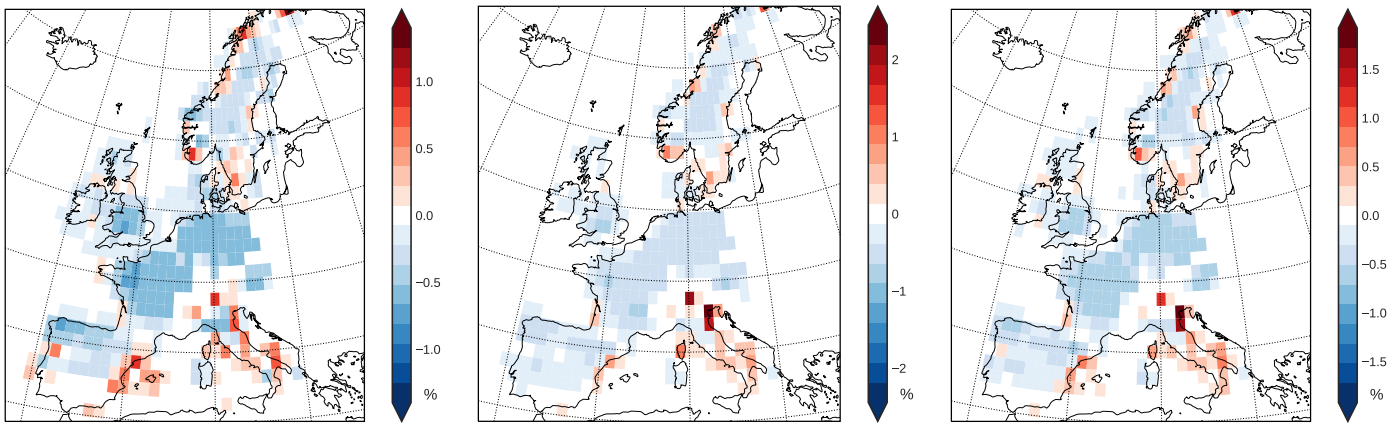

(a) Summer period **(b)** Winter period **(c)** Yearly total

Figure 5.4 – Differenece between the energy production for EC-Earth and ERA-Interim are shown for the summer, winter and yearly total energy production.

5.2 Comparison with HadGEM2-ES

In figure 5.2 the two dimensional histogram of daily energy production for the present day EC-Earth and the HadGEM2-ES dataset is shown. Some difference in the seasonal shape of the data is observed. As some highly unrealistic events are still seen in the HadGEM2-ES dataset, no further analysis will be conducted, until the origin of these interesting events is found.

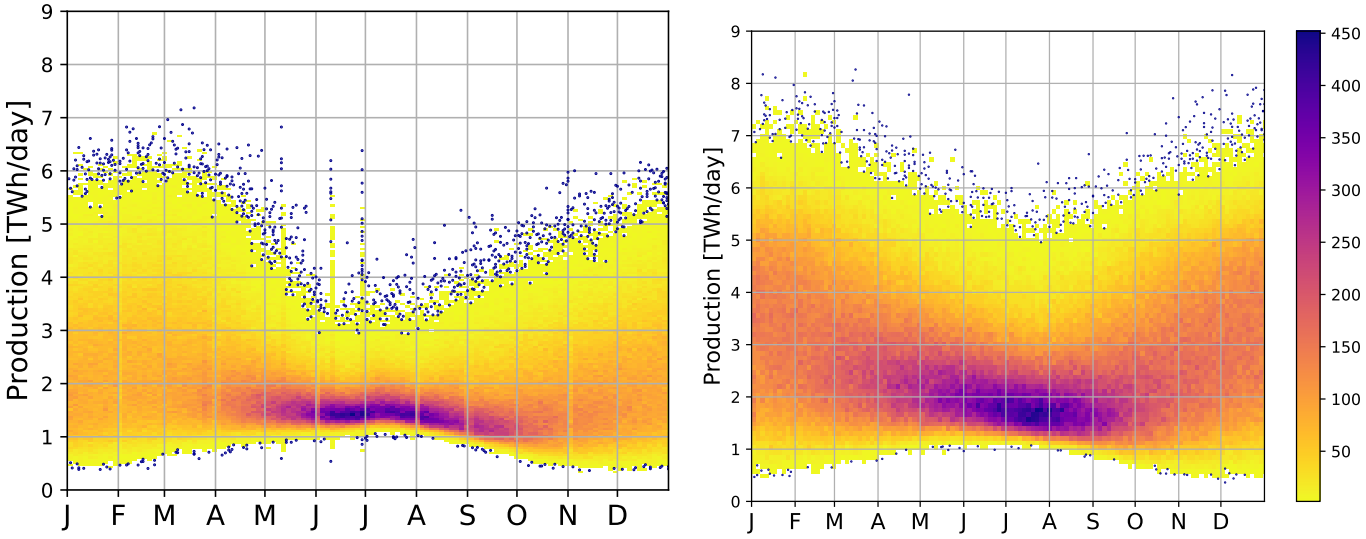

(a) Compound enegy distribution for HadGEM2-ES data

(b) Compound enegy distribution for EC-Earth data

Figure 5.5 – Two dimensional histogram for compound energy production is shown. Coloring as in figure 3.1

5.3 Dependency of the distribution

As the spatial distribution directly determines the selection of high impact events, it is important to study the dependency of the results on the distribution chosen. For this a uniform distribution of renewable energy sources was used. This uniform distribution has the same total installed capacity as the projected distribution, but the wind turbines and solar panels are redistributed over the region. As onshore wind turbines and solar panels are not operational on the sea surface, these are only distributed uniformly over the land region under consideration. The capacity of offshore wind turbines is distributed uniformly over the available shallow seas.

In figure 5.6 the uniform and projected distributions are plotted against each other. Two observation can be made based on figure 5.6. The first observation is that the uniform and projected distributions produce roughly the same amount of electricity on each day in the dataset. The second observation made is that the highest impact events that are under consideration in this study are independent on the specific distribution used. However, the highest compound energy production events for the uniform distribution have a lower production then the projected distribution.

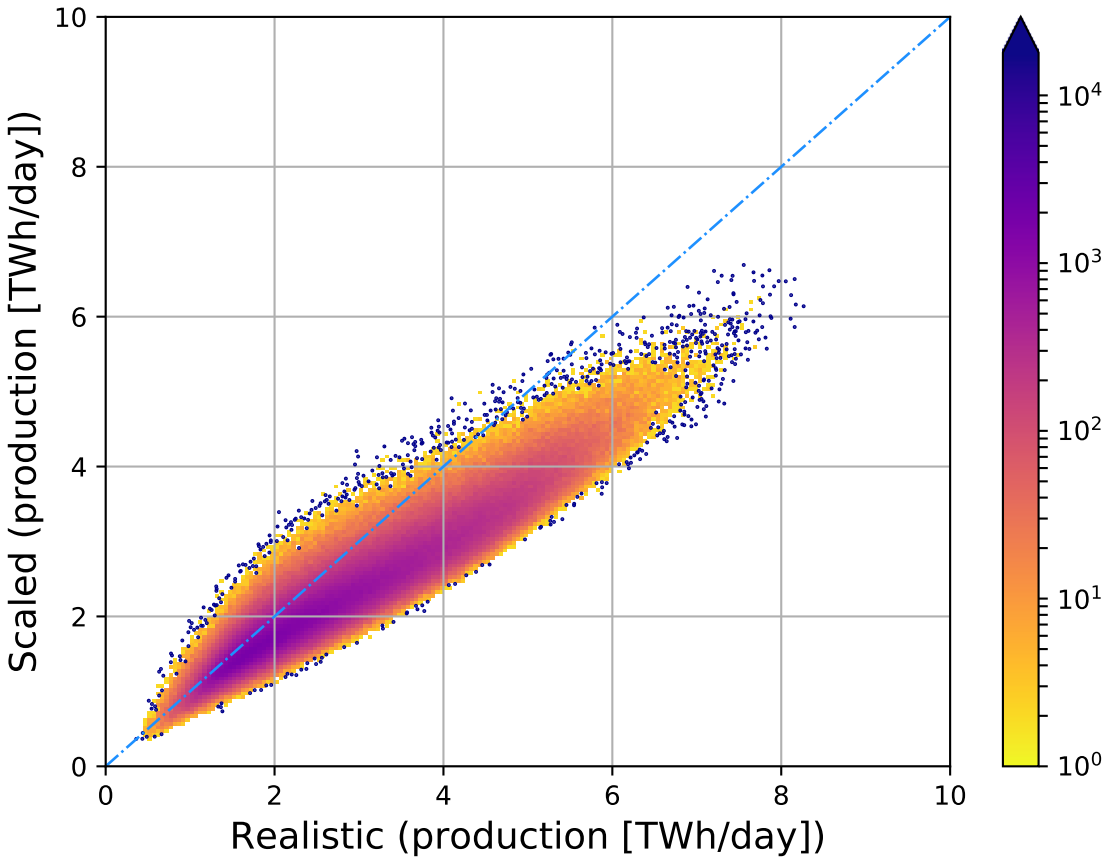

Figure 5.6 – Scatter plot of compound energy production for the two distribution of renewable under consideration. The uniform and projected distribution are called the scaled and realistic distribution here.

5.4 Climate change

When region wide yearly energy production is considered, the return time can be calculated for all days in which a certain energy production threshold is not met. This is shown in figure 5.7 for both the ERA-Interim, the HadGEM2-ES and the EC-Earth dataset. Based on figure **??** the following can be said.

When no changes are assumed in the distribution of renewable energy sources and with a constant temperature dependency of demand, the occurrence of the highest societal impact events for low compound energy production will decrease in a warmer climate. However the highest energy shortage impact events are found to decrease in a warmer climate. It is important to note that the signal found due to climate change is much smaller the intermodel differences in the strength and occurence of the highest societal impact events.

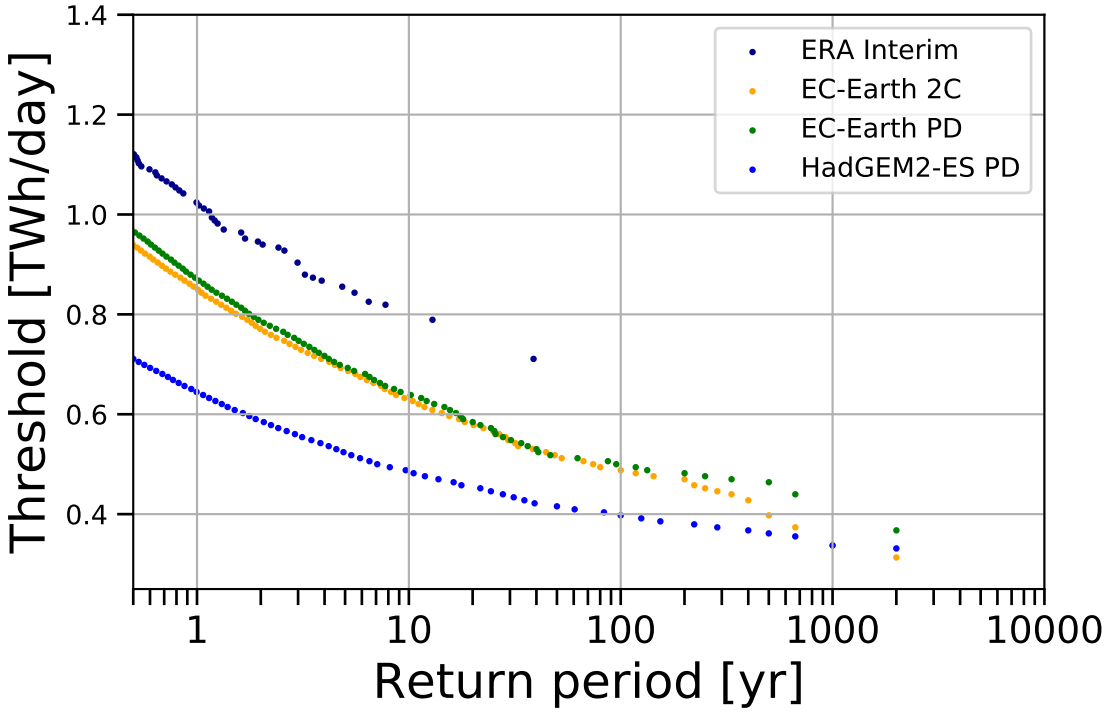

Figure 5.7 – Return time plot for set energy production thresholds. The results of all the models used in this study are shown.

6 Conclusions

Composition of the impact parameters

The daily variability in wind energy production is the main driver for the variability of compound renewable energy production throughout the year, this variability is larger in winter than in summer. Daily average wind energy production is lowest in summer. The lowest wind energy production events are also found in the summer.

Solar energy production shows very little variability throughout the year. Solar energy production is highest in early summer when the days are longer and incoming solar radiation is higher. In winter months the solar energy production can drop to near zero production on some days. However, solar energy production can be regarded as baseload production in the summer months.

Compound energy production has a similar variability throughout the year as wind energy production. Like wind energy production, this variability is highest in winter and smaller in the summer months. The daily mean compound energy production is lowest in summer, even though solar energy production is highest during these months. However, the lowest daily compound energy production events are found in the winter months due to the large variability in production and the baseload production in the summer from solar energy.

Demand of electricity is dependent on meteorological conditions and the rhythm of society. When only the meteorological dependency of demand is considered, a strong non-linear correlation with surface temperature was found for historical demand and temperature from reanalysis data. This historical correlation is used to make projections of possible future energy demand. From late autumn until early spring variability in the daily energy demand of 18% around the mean demand is found. 4% variability around the mean is observed in the summer months. Mean daily energy demand is found to be larger in the winter than in the summer. The highest energy demand events are found in the winter months.

Energy shortage has a similar variability throughout the year as compound energy production. Due to the coupling between higher demand and higher energy production in the winter, the daily mean energy shortage shows very little variability throughout the year. However, as the daily variability is much larger in the winter than in the summer, the highest daily impacts due to energy shortage are found in winter.

High impacts and extreme meteorology

The impact parameters are calculated from meteorological conditions, so when the meteorological conditions are extreme an initial guess could be that these 1-in-10 years extreme meteorological conditions also cause the 1-in-10 years highest societal impacts.

However, of the high-impact compound energy production events only 0.5% was also considered an extreme low wind event. The reason for this is that the lowest mean wind speeds are found in summer, while the high impacts for compound energy production are found in the winter, as in summer solar energy production is always present. Similarly, no extreme event for low incoming solar radiation or extremely low temperature event was found to also be a high-impact compound energy production event.

For the found year high energy shortage impact events, 2% of the events was also considered to be an extreme low temperature event. The origin of this is the strong dependency of energy

demand on temperature, even though the highest energy demand events are not the highest energy shortage events. For both extreme wind speeds and incoming solar radiation events none was also a high energy shortage event.

Meteorological conditions of high-impact events

High impact events due to low energy production are characterized by an extended high pressure system over central Europe during the winter months. The high-pressure system blocks large scale flow over land for most of Western Europe and highly limits flow over coastal regions, reducing the wind speed to below the cut-in of wind turbines. Due to the high-pressure system in central Europe, the high-impact event days are mostly cloudless, and in some regions colder than normal temperatures are observed. The cloudless conditions allow for solar energy production on these days. However, the limited day length and the lower maximum incoming solar radiation in winter highly limit the energy production from solar cells.

Similar to low energy production high-impact events, the highest impact events due to high energy shortage are winter days with a high-pressure system over Europe. There are, however, two distinct differences between them. The first difference is that the high pressure system of the high energy shortage events is less extended and located further northward than the high-pressure system of the lowest energy production. The second distinct difference between them is that for the highest energy shortage events the high-pressure system is accompanied by anomalously cold temperatures over most of Europe. These much lower than normal temperatures drive the demand for energy up.

Prolonged high-impact events

The duration of a high impact event can change the meteorological conditions of a high-impact event as the variability of both compound energy production and energy demand is reduced. The largest reduction in variability is observed in the winter. For both impact measures the reduction is strongest when in the step from a 1-day to a 7-day impact event is considered.

For compound energy production a shift to the summer season for the highest impact events is observed between the 1 and the 14-day highest impact events. No overlap between the 1 and 14-day highest impact events is found. The 7-day prolonged highest impact events are observed in late summer, autumn and winter. The highest prolonged energy shortage events are observed in the winter months. Of the 1 day highest energy shortage events 13.5% is also a 7-day high-impact event and 6% of the 1-day events is also a 14-day high-impact event.

When prolonged events are considered, the relation between high-impact and extreme weather events is amplified for specific cases. More overlapping events are found for combined extreme low wind speed and low compound energy production, and for extreme low temperatures and high energy shortage. No overlapping events were found on a longer time scalefor different combinations of extreme meteorology and high impact.

The meteorological conditions for a 14-day prolonged high impact due to low compound energy production are drastically different than the daily highest impact events as the season of the extremes is shifted from the winter to the summer for the prolonged events. For a 7-day prolonged event the extended high-pressure system is found more northerly and in Scandinavia warmer than normal temperatures are observed.

The meteorological characterization of the highest energy shortage events does not change drastically when prolonged high-impact events are considered. The high-pressure system is a bit more extended when either 7 or 14-day prolonged events are considered. The anomalously cold temperatures are still observed over most of Europe, albeit less extreme.

Bibliography

Akpinar, E. K., and S. Akpinar, 2005: An assessment on seasonal analysis of wind energy characteristics and wind turbine characteristics. *Energy Conversion and Management*, **46 (11-12)**, 1848–1867, doi:10.1016/j.enconman.2004.08.012.

Alexander, K., and S. M. Easterbrook, 2015: The software architecture of climate models: A graphical comparison of CMIP5 and EMICAR5 configurations. *Geoscientific Model Development*, **8 (4)**, 1221–1232, doi:10.5194/gmd-8-1221-2015.

Bessec, M., and J. Fouquau, 2008: The non-linear link between electricity consumption and temperature in Europe: A threshold panel approach. *Energy Economics*, **30 (5)**, 2705–2721, doi:10.1016/j.eneco.2008.02.003.

Bett, P. E., H. E. Thornton, and R. T. Clark, 2013: European wind variability over 140 yr. *Advances in Science and Research*, 51–58, doi:10.5194/asr-10-51-2013, URL http://arxiv.org/abs/1301.4032{%}0Ahttp://dx.doi.org/10.5194/asr-10-51-2013, 1301.4032.

Blanco, H., and A. Faaij, 2018: A review at the role of storage in energy systems with a focus on Power to Gas and long-term storage. *Renewable and Sustainable Energy Reviews*, **81 (July 2017)**, 1049–1086, doi:10.1016/j.rser.2017.07.062, URL http://dx.doi.org/10.1016/j.rser.2017.07.062.

Bloomfield, H. C., 2017: The impact of climate variability and climate change on the GB Power System. Ph.D. thesis, University of Reading, 208 pp., URL http://iopscience.iop.org/article/10.1088/1748-9326/11/12/124025.

Bloomfield, H. C., D. J. Brayshaw, L. C. Shaffrey, P. J. Coker, and H. E. Thornton, 2016: Quantifying the increasing sensitivity of power systems to climate variability. *Environ. Res. Lett.*, **11**, 1–11, doi:10.1088/1748-9326/11/12/124025.

Bloomfield, H. C., D. J. Brayshaw, L. C. Shaffrey, P. J. Coker, and H. E. Thornton, 2018: The changing sensitivity of power systems to meteorological drivers: a case study of Great Britain. *Environmental Research Letters*, **13 (5)**, 054 028, doi:10.1088/1748-9326/aabff9, URL http://stacks.iop.org/1748-9326/13/i=5/a=054028?key=crossref.8f93dc16d12887a06ddc22763f6c7c85.

Brayshaw, D. J., A. Troccoli, R. Fordham, and J. Methven, 2011: The impact of large scale atmospheric circulation patterns on wind power generation and its potential predictability: A case study over the UK. *Renewable Energy*, **36 (8)**, 2087–2096, doi:10.1016/j.renene.2011.01.025, URL http://dx.doi.org/10.1016/j.renene.2011.01.025.

Breton, S. P., and G. Moe, 2009: Status, plans and technologies for offshore wind turbines in Europe and North America. *Renewable Energy*, **34 (3)**, 646–654, doi:10.1016/j.renene.2008.05.040, URL http://dx.doi.org/10.1016/j.renene.2008.05.040.

Cannon, D. J., D. J. Brayshaw, J. Methven, P. J. Coker, and D. Lenaghan, 2015: Using reanalysis data to quantify extreme wind power generation statistics: A 33 year case study in Great Britain. *Renewable Energy*, **75**, 767–778, doi:10.1016/j.renene.2014.10.024, URL http://dx.doi.org/10.1016/j.renene.2014.10.024.

Carrillo, C., A. F. Obando Montaño, J. Cidrás, and E. Díaz-Dorado, 2013: Review of power curve modelling for windturbines. *Renewable and Sustainable Energy Reviews*, **21**, 572–581, doi:10.1016/j.rser.2013.01.012.

Chenni, R., M. Makhlouf, T. Kerbache, and A. Bouzid, 2007: A detailed modeling method for photovoltaic cells. *Energy*, **32 (9)**, 1724–1730, doi:10.1016/j.energy.2006.12.006.

Chiacchio, M., and M. Wild, 2010: Influence of NAO and clouds on long-term seasonal variations of surface solar radiation in Europe. *Journal of Geophysical Research Atmospheres*, **115 (10)**, 1–17, doi:10.1029/2009JD012182.

Collins, W. J., and Coauthors, 2011: Development and evaluation of an Earth-system model – HadGEM2. *Geoscientific Model Development Discussions*, **4 (2)**, 997–1062, doi:10.5194/gmdd-4-997-2011, URL http://www.geosci-model-dev-discuss.net/4/997/2011/.

Cradden, L. C., F. McDermott, L. Zubiate, C. Sweeney, and M. O'Malley, 2017: A 34-year simulation of wind generation potential for Ireland and the impact of large-scale atmospheric pressure patterns. *Renewable Energy*, **106**, 165–176, doi:10.1016/J.RENENE.2016.12.079, URL https://www.sciencedirect.com/science/article/pii/S0960148116311296?via{%}3Dihub.

Davy, R., N. Gnatiuk, L. Pettersson, and L. Bobylev, 2017: Climate change impacts on wind energy potential in the European domain with a focus on the Black Sea. *Renewable and Sustainable Energy Reviews*, **81 (May)**, 1–8, doi:10.1016/j.rser.2017.05.253, URL http://linkinghub.elsevier.com/retrieve/pii/S1364032117308997https://www.sciencedirect.com/science/article/pii/S1364032117308997.

Dee, D. P., and Coauthors, 2011: The ERA-Interim reanalysis: Configuration and performance of the data assimilation system. *Quarterly Journal of the Royal Meteorological Society*, **137 (656)**, 553–597, doi:10.1002/qj.828.

Díaz-González, F., A. Sumper, O. Gomis-Bellmunt, and R. Villafáfila-Robles, 2012: A review of energy storage technologies for wind power applications. *Renewable and Sustainable Energy Reviews*, **16 (4)**, 2154–2171, doi:10.1016/j.rser.2012.01.029, URL http://dx.doi.org/10.1016/j.rser.2012.01.029.

Emeis, S., and M. Turk, 2007: Comparison of Logarithmic Wind Profiles and Power Law Wind Profiles and their Applicability for Offshore Wind Profiles. Tech. Rep. 1, Institut fur Meteorologie und Klimaforschung, Karlsruhe, 1–4 pp. doi:10.1007/978-3-540-33866-6_11, URL http://dx.doi.org/10.1007/978-3-540-33866-6{_}11.

EPRI, 2010: Electric Energy Storage Technology Options: A White Paper Primer on Applications, Costs and Benefits. *Epri*, 1–170, doi:EPRI1020676, URL http://large.stanford.edu/courses/2012/ph240/doshay1/docs/EPRI.pdf.

European Environment Agency, 2009: *Europe's Onshore and Offshore Wind Energy Potential: An Assessment of Environmental and Economic Constraints*. EEA-TR–6/2009, Publications Office, URL https://books.google.nl/books?id=RqQsmQEACAAJ.

Ferreira, H. L., R. Garde, G. Fulli, W. Kling, and J. P. Lopes, 2013: Characterisation of electrical energy storage technologies. *Energy*, **53**, 288–298, doi:10.1016/j.energy.2013.02.037, URL http://dx.doi.org/10.1016/j.energy.2013.02.037.

Forsythe, W. C., E. J. Rykiel, R. S. Stahl, H. i. Wu, and R. M. Schoolfield, 1995: A model comparison for daylength as a function of latitude and day of year. *Ecological Modelling*, **80 (1)**, 87–95, doi:10.1016/0304-3800(94)00034-F.

Gabrielli, P., M. Gazzani, E. Martelli, and M. Mazzotti, 2018: Optimal design of multi-energy systems with seasonal storage. *Applied Energy*, **219 (October 2017)**, 408–424, doi:10.1016/j.apenergy.2017.07.142, URL https://doi.org/10.1016/j.apenergy.2017.07.142.

Giebel, G., 2000: Equalizing effects of the wind energy production on Northern Europe from reanalysis data. Tech. Rep. May, Risø National Laboratory, Roskilde.

Grams, C. M., R. Beerli, S. Pfenninger, I. Staffell, and H. Wernli, 2017: Balancing Europe's wind-power output through spatial deployment informed by weather regimes. *Nature Climate Change*, **7 (8)**, 557–562, doi:10.1038/NCLIMATE3338.

Hazeleger, W., and Coauthors, 2010: EC-Earth: A seamless Earth-system prediction approach in action. *Bulletin of the American Meteorological Society*, **91 (10)**, 1357–1363, doi:10.1175/2010BAMS2877.1.

Hazeleger, W., and Coauthors, 2012: EC-Earth V2.2: Description and validation of a new seamless earth system prediction model. *Climate Dynamics*, **39 (11)**, 2611–2629, doi:10.1007/s00382-011-1228-5.

Hedegaard, K., and P. Meibom, 2012: Wind power impacts and electricity storage - A time scale perspective. *Renewable Energy*, **37 (1)**, 318–324, doi:10.1016/j.renene.2011.06.034, URL http://dx.doi.org/10.1016/j.renene.2011.06.034.

Hsu, S. A., E. a. Meindl, and D. b. Gilhousen, 1994: Determining the Power-Law Wind-Profile under Near-Neutral Stability Conditions at Sea. Journal of Applied meteorology, 8 pp.

Hueging, H., R. Haas, K. Born, D. Jacob, and J. G. Pinto, 2013: Regional changes in wind energy potential over Europe using regional climate model ensemble projections. *Journal of Applied Meteorology and Climatology*, **52 (4)**, 903–917, doi:10.1175/JAMC-D-12-086.1.

International Energy Agency, 2017: World Energy Outlook 2017. Tech. rep., International Energy Agency. doi:10.1016/0301-4215(73)90024-4, 978-92-64-26494-6.

Jerez, S., F. Thais, I. Tobin, M. Wild, A. Colette, P. Yiou, and R. Vautard, 2015: The CLIMIX model: A tool to create and evaluate spatially-resolved scenarios of photovoltaic and wind power development. *Renewable and Sustainable Energy Reviews*, **42**, 1–15, doi:10.1016/j.rser.2014.09.041, URL http://dx.doi.org/10.1016/j.rser.2014.09.041.

Jerez, S., R. M. Trigo, S. M. Vicente-Serrano, D. Pozo-VáZquez, R. Lorente-Plazas, J. Lorenzo-Lacruz, F. Santos-Alamillos, and J. P. MontáVez, 2013: The impact of the north atlantic oscillation on renewable energy resources in Southwestern Europe. *Journal of Applied Meteorology and Climatology*, **52 (10)**, 2204–2225, doi:10.1175/JAMC-D-12-0257.1.

Kaldellis, J. K., and D. Zafirakis, 2011: The wind energy (r)evolution: A short review of a long history. *Renewable Energy*, **36 (7)**, 1887–1901, doi:10.1016/j.renene.2011.01.002.

Koch, H., S. Vögele, F. F. Hattermann, and S. Huang, 2015: The impact of climate change and variability on the generation of electrical power. *Meteorologische Zeitschrift*, doi:10.1127/metz/2015/0530.

Koster, R., 2018: Grilligheid zon en windenergie. Hilversum, URL https://nos.nl/artikel/2230510-grilligheid-zon-en-wind-bedreigt-stabiliteit-elektriciteitsnet.html, 1 pp.

Mathew, S., 2007: *Wind energy: Fundamentals, resource analysis and economics*. Springer Berlin Heidelberg, 1–246 pp., doi:10.1007/3-540-30906-3, arXiv:1011.1669v3.

Mavromatakis, F., G. Makrides, G. Georghiou, A. Pothrakis, Y. Franghiadakis, E. Drakakis, and E. Koudoumas, 2010: Modeling the photovoltaic potential of a site. *Renewable Energy*, **35 (7)**, 1387–1390, doi:10.1016/j.renene.2009.11.010, URL http://dx.doi.org/10.1016/j.renene.2009.11.010.

Monforti, F., M. Gaetani, and E. Vignati, 2016: How synchronous is wind energy production among European countries? Elsevier, 1622–1638 pp., doi:10.1016/j.rser.2015.12.318.

Moral-Carcedo, J., and J. Vicéns-Otero, 2005: Modelling the non-linear response of Spanish electricity demand to temperature variations. *Energy Economics*, **27 (3)**, 477–494, doi:10.1016/j.eneco.2005.01.003.

Morice, C. P., J. J. Kennedy, N. A. Rayner, and P. D. Jones, 2012: Quantifying uncertainties in global and regional temperature change using an ensemble of observational estimates: The HadCRUT4 data set. *Journal of Geophysical Research Atmospheres*, **117 (8)**, 1–22, doi:10.1029/2011JD017187.

NOS, 2018: NOS Journaal 05-05-2018. URL https://www.npostart.nl/nos-journaal/05-05-2018/POW{_}03689510{#}dd6d4c70f.

Pardo, A., V. Meneu, and E. Valor, 2002: Temperature and seasonality influences on Spanish electricity load. *Energy Economics*, **24 (1)**, 55–70, doi:10.1016/S0140-9883(01)00082-2.

Pozo-Vázquez, D., J. Tovar-Pescador, S. R. Gámiz-Fortis, M. J. Esteban-Parra, and Y. Castro-Díez, 2004: NAO and solar radiation variability in the European North Atlantic region. *Geophysical Research Letters*, **31 (5)**, n/a–n/a, doi:10.1029/2003GL018502, URL http://doi.wiley.com/10.1029/2003GL018502.

Pryor, S. C., R. J. Barthelmie, and J. T. Schoof, 2006: Inter-annual variability of wind indices across Europe. *Wind Energy*, **9 (1-2)**, 27–38, doi:10.1002/we.178.

Ravestein, P., G. van der Schrier, R. Haarsma, R. Scheele, and M. van den Broek, 2018: Vulnerability of European intermittent renewable energy supply to climate change and climate variability.

Sanchis, G. e.-H., 2015: Europe' s future secure and sustainable electricity infrastructure. Tech. Rep. 308908, e-Highway2050, Europe2020, 52 pp. URL https://www.entsoe.eu/news-events/events/Pages/Events/e-Highway2050-Final-Conference.aspx.

Staffell, I., and S. Pfenninger, 2016: Using bias-corrected reanalysis to simulate current and future wind power output. *Energy*, **114**, 1224–1239, doi:10.1016/j.energy.2016.08.068, URL http://dx.doi.org/10.1016/j.energy.2016.08.068.

Staffell, I., and S. Pfenninger, 2018: The increasing impact of weather on electricity supply and demand. *Energy*, **145**, doi:10.1016/j.energy.2017.12.051.

Staffell, I., and M. Rustomji, 2016: Maximising the value of electricity storage. *Journal of Energy Storage*, **8**, 212–225, doi:10.1016/j.est.2016.08.010, URL http://dx.doi.org/10.1016/j.est.2016.08.010.

TamizhMani, G., L. Ji, Y. Tang, and L. Petacci, 2003: Photovoltaic module thermal/wind performance: Long -Term Monitoring and Model Development For Energy Rating. *Proc. NCPV and Solar Program . . .*, 936–939, URL http://scholar.google.com/scholar?hl=en{&}btnG=Search{&}q=intitle:Photovoltaic+module+thermal/wind+performance:{#}4.

Terasvirta, T., 1994: Specification , Estimation , and Evaluation of Smooth Transition Autoregressive Models. *Journal of the American Statistical Association*, **89 (425)**, 208–218, doi:10.2307/2291217, URL www.jstor.org/stable/2291217.

Thornton, H. E., B. J. Hoskins, and A. A. Scaife, 2016: The role of temperature in the variability and extremes of electricity and gas demand in Great Britain . *Environmental Research Letters*, **11 (11)**, 1–25, doi:10.1088/1748-9326/11/11/114015, URL http://dx.doi.org/10.1088/1748-9326/11/11/114015.

Tobin, I., W. Greuell, S. Jerez, F. Ludwig, R. Vautard, M. M. van Vliet, F.-M. Bréon, and F. Breon, 2018: Vulnerabilities and resilience of European power generation to 1.5C, 2C and 3C warming. *Environmental Research Letters*, doi:10.1088/1748-9326/aab211, URL https://doi.org/10.1088/1748-9326/aab211http://iopscience.iop.org/article/10.1088/1748-9326/aab211.

Tobin, I., and Coauthors, 2016: Climate change impacts on the power generation potential of a European mid-century wind farms scenario. *Environmental Research Letters*, **11 (3)**, 34 013, doi: 10.1088/1748-9326/11/3/034013, URL http://dx.doi.org/10.1088/1748-9326/11/3/034013.

Valor, E., V. Meneu, and V. Caselles, 2001: Daily Air Temperature and Electricity Load in Spain. *Journal of Applied Meteorology*, **40 (8)**, 1413–1421, doi:10.1175/1520-0450(2001)040<1413:DATAEL>2.0.CO;2, URL http://journals.ametsoc.org/doi/abs/10.1175/1520-0450{%}282001{%}29040{%}3C1413{%}3ADATAEL{%}3E2.0.CO{%}3B2.

van der Wiel, K., F. M. Selten, R. Bintanja, R. Blackport, and J. A. Screen, 2018: More accurate assessment of climate induced impacts. *Bulletin of the American Meteorological Society*, **(in review)**.

Zscheischler, J., and Coauthors, 2018: Future climate risk from compound events. *Nature Climate Change*, 1, doi:10.1038/s41558-018-0156-3, URL http://www.nature.com/articles/s41558-018-0156-3.

Word of Thanks

A master thesis is not a little project that you finish in a short time, that will be archived to prove your competence as a researcher. A master thesis is like the current of a wild river down the hill of life, it accumulates grains of knowledge on the way and grows steadily, based on the input of others until it is a foaming mass of water. When it has grown this foaming river might become strong enough to start to carve its own path and careful guidance is needed to prevent it from spiralling out of control. Luckily in life you are not alone. With the help of a team, timber might be felled on the riverbanks and carried down by the river to supply the paper factories down in the valleys.

During the work on my thesis I had the luck to have the support of a large group of people that helped me in wrangling the mountain river. My gratitude goes out to them, as without them I would not have been able to guide the turmoil that was my research into a canal that can be used in the future to carry the logs to the paper factories.

For trusting me with her ideas and her endless moments of guidance, I would like to thank Karin, my supervisor and guide to the wriggling stream that lies at the basis of my research. Thank you for being patient with me and my continued tomfoolery and antics in coding and thank you above all for the talks we had about career- and life goals.

For his time, patience and trust in my external project, I would like to thank my supervisor Aarnout van Delden. You were open to my excursion to the boundaries of Climate Physics and allowed me to follow my own path, thank you.

For their faith in my research and their time to answer my questions I would like to thank Franks Selten and Machteld van den Broek. I would also like to thank Bas van Zuijlen, for entrusting me with the results of his research and his projected distribution of renewable energy sources.

For the time she spent explaining the field of Energy Science to me, as well as making me understand the faults in my logic, I want to thank Monique Dorresteijn. You supplied me with your knowledge and interest into this research and without your beta stage proofreading, my thesis and research would undoubtedly have contained grave errors in modelling renewables.

For teaching me some handY words in Greek, discussing research and brainstorming about ways to solve problems we found in our streams of research, I would like to thank Nomikos, Eleftheris and Dimitris, my roommates at KNMI. During the moments I got stuck, you helped me rethink the problem and to approach it from a new direction.

During my thesis I had the good fortune to work with a large group of people at KNMI without whom I would not have come to where I am now. My sincere thanks to Folmer Krikken, for taking the time to discuss the quirks of Python and Xarray with me. My gratitude also goes out to Geert-Jan van Oldenburgh, who always supplied me with the latest data from reanalysis data sets and insight in properties of the weather of the previous month. Thanks are also due to all those in the Python Working Group at KNMI, for discussions on the use of Python in climate research.

Lastly, I would like to thank my girlfriend, fiancé and wife to be. Shawn, without your support during my research I would not have made it as far as I have and without your proofreading I would not have been able to finish my thesis with the results I have obtained. Thank you for listening when I was stuck, being there when I needed cheering on and for showing me the light when all I could see was darkness.